**SANDIA REPORT**
SAND2013-7962
Unlimited Release
Printed September 2013

# Feasibility of Preparing Patterned Molybdenum Coatings on Bismuth Telluride Thermoelectric Modules

Pylin Sarobol, Aaron C. Hall, Stephen S. Miller, Marlene E. Knight, William S. LePage, Catherine E. Sobczak, and Daniel E. Wesolowski

Prepared by
Sandia National Laboratories
Albuquerque, New Mexico 87185 and Livermore, California 94550

Sandia National Laboratories is a multi-program laboratory managed and operated by Sandia Corporation, a wholly owned subsidiary of Lockheed Martin Corporation, for the U.S. Department of Energy's National Nuclear Security Administration under contract DE-AC04-94AL85000.

Approved for public release; further dissemination unlimited.

Sandia National Laboratories

Issued by Sandia National Laboratories, operated for the United States Department of Energy by Sandia Corporation.

**NOTICE:** This report was prepared as an account of work sponsored by an agency of the United States Government. Neither the United States Government, nor any agency thereof, nor any of their employees, nor any of their contractors, subcontractors, or their employees, make any warranty, express or implied, or assume any legal liability or responsibility for the accuracy, completeness, or usefulness of any information, apparatus, product, or process disclosed, or represent that its use would not infringe privately owned rights. Reference herein to any specific commercial product, process, or service by trade name, trademark, manufacturer, or otherwise, does not necessarily constitute or imply its endorsement, recommendation, or favoring by the United States Government, any agency thereof, or any of their contractors or subcontractors. The views and opinions expressed herein do not necessarily state or reflect those of the United States Government, any agency thereof, or any of their contractors.

Printed in the United States of America. This report has been reproduced directly from the best available copy.

Available to DOE and DOE contractors from
U.S. Department of Energy
Office of Scientific and Technical Information
P.O. Box 62
Oak Ridge, TN 37831

Telephone: (865) 576-8401
Facsimile: (865) 576-5728
E-Mail: reports@adonis.osti.gov
Online ordering: http://www.osti.gov/bridge

Available to the public from
U.S. Department of Commerce
National Technical Information Service
5285 Port Royal Rd.
Springfield, VA 22161

Telephone: (800) 553-6847
Facsimile: (703) 605-6900
E-Mail: orders@ntis.fedworld.gov
Online order: http://www.ntis.gov/help/ordermethods.asp?loc=7-4-0#online

SAND2013-7962
Unlimited Release
Printed September 2013

# Feasibility of Preparing Patterned Molybdenum Coatings on Bismuth Telluride Thermoelectric Modules

Pylin Sarobol, Aaron C. Hall, Stephen S. Miller, Marlene E. Knight,
William S. LePage, Catherine E. Sobczak, and Daniel E. Wesolowski*

Coatings and Surface Science, 01832
*Emerging Power Sources R&D, 02545

Sandia National Laboratories
P.O. Box 5800
Albuquerque, New Mexico 87185

Abstract

Molybdenum electrical interconnects for thermoelectric modules were produced by air plasma spraying a 30µm size molybdenum powder through a laser-cut Kapton tape mask. Initial feasibility demonstrations showed that the molybdenum coating exhibited excellent feature and spacing retention (~170µm), adhered to bismuth-telluride, and exhibited electrical conductivity appropriate for use as a thermoelectric module interconnect. A design of experiments approach was used to optimize air plasma spray process conditions to produce a molybdenum coating with low electrical resistivity. Finally, a molybdenum coating was successfully produced on a full-scale thermoelectric module. After the addition of a final titanium/gold layer deposited on top of the molybdenum coating, the full scale module exhibited an electrical resistivity of 128Ω, approaching the theoretical resistivity value for the 6mm module leg of 112Ω.

Importantly, air plasma sprayed molybdenum did not show significant chemical reaction with bismuth-telluride substrate at the coating/substrate interface. The molybdenum coating microstructure consisted of lamellar splats containing columnar grains. Air plasma sprayed molybdenum embedded deeply (several microns) into the bismuth-telluride substrate, leading to good adhesion between the coating and the substrate. Clusters of round pores (and cracks radiating from the pores) were found immediately beneath the molybdenum coating. These pores are believed to result from tellurium vaporization during the spray process where the molten molybdenum droplets (2623°C) transferred their heat of solidification to the substrate at the moment of impact. Substrate cooling during the molybdenum deposition process was recommended to mitigate tellurium vaporization in future studies.

## ACKNOWLEDGMENTS

The authors would like to acknowledge Ronald Goeke for conducting resistivity measurements, Adrian Wagner for mask and fixture fabrication, Michael Rye for FIB/EDS analysis, and Daniel Wesolowski for valuable discussions.

# CONTENTS

1. Introduction ..... 11

2. Experimental Procedures ..... 13
   2.1. Molybdenum Coating Preparation ..... 13
   2.2. Mask Preparation ..... 14
   2.3. Electrical Resistivity Measurement ..... 17
   2.4. Microstructural Examination ..... 18
   2.5. Particle Temperature, Velocity, and Diameter Measurement ..... 18

3. Phase I - Feasibility Demonstration ..... 19
   3.1. Masking Feasibility ..... 19
      3.1.1. Coating Edge and Feature Retention ..... 22
   3.2. Coating Electrical Properties ..... 24
   3.3. Coating Microstructure ..... 24
   3.4. Phase I Feasibility Demonstration Summary ..... 31

4. Phase II - APS Process Optimization ..... 33
   4.1. Designed Experiment (DOE) for APS Mo Process Optimization ..... 33
      4.1.1. Effects of Arc Current, Total Plasma Gas Flow, and Standoff Distance on Particle Temperature (Tp) and Velocity (Vp) ..... 35
      4.1.2. Effects of Arc Current, Total Plasma Gas Flow, Standoff Distance on Sheet Resistance ..... 37
      4.1.3. Optimal APS coatings on N and P-type Bismuth Telluride ..... 40
   4.2. Phase II Coating Process Optimization Summary ..... 47

5. Phase III – Demonstration of An APS Mo Interconnect on Thermoelectric Modules 49
   5.1. Second DOE for APS Process Optimization ..... 49
   5.2. Preparation of Mo Coatings on Thermoelectric Modules ..... 50
      5.2.1. Stack Fixture Design for APS Coating ..... 50
      5.2.2. Preparing an APS Mo Coating on Thermoelectric Modules ..... 52
      5.2.3. Thermoelectric Module Circuit Testing ..... 52
      5.2.4. Circuit Repair ..... 52
   5.3. Circuit Testing Results ..... 53
   5.4. Microstructure of Air Plasma Spray Coating on Ti/Au Layer ..... 55
   5.5. Phase III Thermoelectric Module Coating Summary ..... 57

6. Summary and Recommendations ..... 59

7. References ..... 60

8. Distribution ..... 62

# FIGURES

Figure 1: TriplexPro®-210 air plasma spray torch (Sulzer-Metco, Inc. Westbury, NY) used to prepare molybdenum coatings at Sandia's Thermal Spray Research Laboratory. ..... 13

Figure 2: Schematic (left) and image (right) of a TriplexPro®-210 air plasma spray torch. The three cathode extended arc design of the Triplex provides an extremely stable high energy plasma that can effectively spray a wide range of materials. [5]. ..... 13

Figure 3: Mask Design with dimensions. The two design were used for opposite ends of the thermoelectric stack. ..... 15
Figure 4: An edge of the mask cut from Kapton sheet prior to spraying. The mask is surrounded by silicone tape (red material) and aluminum tape (white material) used to secure it during spraying. ..... 15
Figure 5: As-received laser-cut mask prepared using carbon-filled Kapton tape on Mylar. The Kapton tape contains Carbon, providing the brown color to the tape. Note the disrupted edges (shown by arrows) on the mask already existed prior to spraying. Due to the line-of-sight nature of the thermal spray process, these non-uniformities in the mask will likely lead to a coating with poor feature edge retention and spacing. ..... 16
Figure 6: A) Au-coated Kapton mask partially attached to an $Al_2O_3$ substrate with silicone tape. The Au coating was expected to protect the Kapton mask from the Molybdenum droplets. B) Fully masked and taped substrate prior to coating. Only the patterned area of the Kapton mask is exposed to the Molybdenum droplet stream. ..... 16
Figure 7: Fully masked $Al_2O_3$ substrate (with silicone and aluminum tapes) attached to a rotary fixture ready to be plasma sprayed with Molybdenum. The air knife seen in the left foreground of this image is positioned ~90° from the spray plume. This allowed the coated part to rapidly pass through the plasma and then immediately through the cooling air jet as the fixture rotated. ..... 17
Figure 8: Two images of the Au coated Kapton mask after spraying with 8 passes of Mo (~70 µm size powder). The Mo droplets are clearly melting the Au sputter coating and causing it to delaminate from the Kapton substrate. No damage to the Kapton edges or the Kapton itself is observed on this mask. ..... 21
Figure 9: Two images showing masks cut from Kapton sheet without Au coating after spraying with 24 passes of Mo (~70 µm size powder). No significant damage to the mask is observed. Mo droplets have clearly left pock marks on the mask surface but they have not burned the mask or caused loss of edges or features. The Mo coating can clearly be seen beneath the mask. ..... 21
Figure 10: Two images of the masks cut from carbon filled Kapton tape after spraying with Mo (~10 µm size powder). No damage to the Kapton edges or the Kapton itself is apparent on this mask. ..... 22
Figure 11: Initial attempt at preparing a patterned Mo coating (8 passes) on an $Al_2O_3$ substrate resulted in poor edge and feature retention. Splashing of Mo beneath the mask can be seen. This splashing and the large Mo particle size used (~70 µm) contributed to poor feature definition. ..... 23
Figure 12: Improved Mo coating (~10µm powder, 20 passes) on an $Al_2O_3$ substrate with reduced splashing and excellent feature definition. Some missing edges due to residue on the laser-cut Kapton tape masks were occasionally observed. ..... 23
Figure 13: Mo coating (10µm powder size, 4 passes) on $Bi_2Te_3$ substrate. A) SEM image showing the Mo coated areas (light rectangular regions) and the substrate (dark areas). The coating appears rough and non-uniform. Adhesive residue is marked with the white arrow. B) High magnification SEM image showing a Mo coated region. Molybdenum splats (dotted blue arrows) and larger Mo particles (solid black arrows) were observed. ..... 25
Figure 14: High magnification SEM images showing the Mo coating (10µm powder size, 4 passes) on Bi2Te3 substrate. ..... 25

Figure 15: EDS maps showing the Mo coating surface. Bi (yellow), Te (red), and Se (green) are present in the substrate. Mo (cyan) is present in the coating. The arrows in the figures point to the same features. ..... 26
Figure 16: SEM images showing FIB cross-section of Mo (10µm powder size, 4 passes) on $Bi_2Te_3$ (A), revealing pores in the substrate (B,C), at the coating/substrate interface (C,D), and at splat boundaries within the coating (E,F). Mo coating exhibited dendritic solidification (C-F)..... 27
Figure 17: EDS analysis of the Mo coating cross section (10µm powder size, 4 passes). Distinct regions can be seen including: the Pt protective layer on the coating surface, the Mo coating, as well as Bi and Te (and Se) in the $Bi_2Te_3$ substrate. No significant Mo/$Bi_2Te_3$ mixing was observed at the interface..... 28
Figure 18: Polished cross section of the unsprayed $Bi_2Te_3$ substrate. This higher magnification picture still showed signs of pre-existing voids and cracks right below the substrate surface, along the grain boundaries. ..... 29
Figure 19: Polished cross section of the sprayed Mo (70µm powder size) on $Bi_2Te_3$ substrate. The coating/substrate interface appeared wavy contains voids. Note that cracks are present immediately below the coating-substrate interface, along the grain boundaries the $Bi_2Te_3$. ..... 29
Figure 20: Polished cross section showing the Mo (70µm powder size) coating on the $Bi_2Te_3$ substrate. The transition between the sprayed and masked regions can be seen at the right side of the image. Notice that the uncoated substrate on the right-hand side is much smoother (more planar) compared to the substrate beneath the Mo sprayed coating on the left-hand side of the image..... 30
Figure 21: Polished cross section showing sprayed Mo (70µm powder size) coating on the $Bi_2Te_3$ substrate. This higher magnification image showed signs of possible Mo-$Bi_2Te_3$ mechanical interaction at the wavy coating/substrate interface. Subsequent layers of Mo showed the elongated grains "splats" containing columnar structures, typical of coatings prepared using APS. Note the cracks immediately below the interface, along the grain boundaries of the $Bi_2Te_3$ substrate..... 30
Figure 22: Effects of arc current, total plasma gas flow, and standoff distance on particle temperature and velocity..... 36
Figure 23: Main effects of arc current, total plasma gas flow, and standoff distance as well as their interactions on sheet resistance, calculated using the data obtained from the DOE in MiniTab..... 38
Figure 24: Cube plot showing sheet resistance (ohms/square) as a function of arc current, total plasma gas flow, and standoff distance. The point with the lowest sheet resistance value is at the edge of the DOE space, where the APS conditions are the least energetic (lowest arc current, lowest total plasma gas flow and longest standoff distance). Addition exploration of lower energy process conditions is needed..... 39
Figure 25: Mo coatings (36µm powder size, 10 passes) produced using the optimized APS process parameters on the N-type (left) and P-type (right) Bi-Te coupons..... 40
Figure 26: SEM images of the Mo coating on an N-type Bi-Te substrate. The substrate and coating surface are rough. The coating surface is non-uniform. A) Image showing good feature and edge retentions of the coating. Some large Mo droplets can also be seen in the coating. B) High magnification SEM image showing splats and condensation at the coating surface ..... 41

Figure 27: A) SEM image of FIB cross-section of the Mo coating on an N-type Bi-Te substrate. B) High magnification SEM image of the far left corner of the cross-section. This Mo structure is likely from one or two splats. It penetrated deep into the substrates and exhibited dendritic solidification mode. ..... 41
Figure 28: EDS analysis of FIB cross section of Mo on N-type Bi-Te substrate, showing distinct regions including: Pt protective layer on the coating surface, Mo in the coating, and Bi, Te, and Se in the substrate. No significant mixing was observed at the coating substrate interface..... 42
Figure 29: Back-scattered electron images of polished coating cross-sections showing Mo on an N-Type Bi-Te substrate. The coating is approximately 10±5µm thick. The bare substrate had sub-surface cracks and voids (bottom left picture) prior to Mo deposition. The coating (top and bottom right images) exhibits characteristic lamellar structure with columnar grains inside the Mo lamelle. This is typical of coatings produced by thermal spray process. As before, voids were found immediately beneath the coating. These are believed to arise from gas bubbles produced by Te vaporization during the Mo deposition process. ..... 43
Figure 30: SEM images showing the Mo coating on a P-type Bi-Te substrate. A) SEM image showing a top view of the coating. Exposed substrate areas with pre-existing cracks can be seen. The cross-section was performed in the area indicated by the box in the left image. B) The cross-section showing Mo splats penetration, deep into the substrate. Mo exhibited dendritic solidification. Voids are observed in the Mo coating as well as at the splat boundaries, the coating/substrate interface, and in the substrate.. ..... 44
Figure 31: EDS maps taken from the FIB cross section of the Mo coating on the P-type Bi-Te substrate, showing distinct regions including: the Pt protective layer on the coating surface, Mo in the coating, and Bi, Te, and Sb in the substrate. No significant mixing was observed at the coating substrate interface..... 45
Figure 32: Back-scattered electron images of polished metallographic cross-sections showing the Mo coating on a P-Type Bi-Te substrate. The bare substrate had sub-surface cracks and numerous voids (bottom left picture) prior to coating deposition. The coating (top and bottom right images) exhibits a lamellar microstructure characteristic of sprayed coatings. Voids were found within the splats and at the splat boundaries. The top right picture also shows a particle that solidified dendritically prior to reaching the substrate. Voids were found immediately under the coating. These are believed to be gas bubbles formed by Te vaporization during the spray process..... 46
Figure 33: 3D Solid Works drawing of the fixture designed to hold three thermoelectric stacks, shaped to fit into TSRL's APS substrate holder. ..... 50
Figure 34: Multiple views of the fixture designed to hold three thermoelectric stacks, shaped to fit into TSRL's APS substrate holder. ..... 51
Figure 35: Final assembly of the fixture. These two images were taken after spraying..... 51
Figure 36: Thermoelectric Stack #22 coated with Mo. The left image is the front side and the right image is the back side of the stack. Macro-voids (dark spots) in the cement matrix can be seen. The Mo features were well defined and distinct. The resistance after Ti-Au deposition circuit repair was measured to be 127.8Ω, approaching the theoretical resistance of 112Ω for a module with 6 mm long legs..... 53

Figure 37: Thermoelectric Stack #20 coated with Mo. The left image is the front side and the right image is the back side of the stack. Macro-voids (dark spots) in the cement matrix can be seen. There were overlapping features in the Mo coating. The resistance after Ti-Au deposition circuit repair was measured to be 47.5Ω due to overlapping features. ..... 54
Figure 38: SEM images of CoNiCrAlY coating and FIB cross-section of the CoNiCrAlY coating (22µm powder size, 13 passes) on sputtered Ti/Au (light-colored layer) on Bi-Te substrate. ..... 55
Figure 39: EDS analysis of a CoNiCrAlY cross section (22.027µm powder size, 13 passes) on sputtered Ti/Au over a Bi-Te substrate, showing distinct regions of sputtered Au layer, CoNiCrAlY coating, as well as Bi and Te in the substrate. No embedding or significant mixing between the Au and the Bi-Te were observed at the interface. ..... 56

## TABLES

Table 1: Process parameters and set points used to prepare Molybdenum coatings for initial mask evaluation. Masks cut from clean Kapton sheet (Set Point 1), Au-coated Kapton sheet (Set Point 1), and carbon filled Kapton tape (Set Point 2) were placed on $Al_2O_3$ substrates and coated using these conditions. The same parameters were also used to prepare coatings onto bismuth-telluride substrates for metallographic examination.....20
Table 2: Full factorial design used for the Mo Phase II DOE. Arc Current, Total Plasma Gas Flow and Standoff Distance were varied. Argon Flow and He Flow were calculated using a fixed Ar:He ratio of 1.75:1.....33
Table 3: Process parameters and set points held constant throughout the Phase II DOE.....34
Table 4: DOE Results: Vp, Tp, Dp, Kapton Survival, and Mo Sheet Resistance .....35
Table 5: ANOVA analysis for sheet resistance .....37
Table 6: Results on Vp, Tp, Dp and Electrical Resistivity from refined DOE in Phase III .....49
Table 7: Column-by-column electrical resistance of as-sprayed Mo coatings from the first set of the thermoelectric stacks, module #22 and #20. The ideal resistance value across a column is ~20Ω.....53

# NOMENCLATURE

| | |
|---|---|
| A | Amps |
| Al | Aluminum |
| $Al_2O_3$ | Aluminum oxide |
| APS | Air Plasma Spray |
| Ar | Argon |
| Au | Gold |
| Bi | Bismuth |
| C | Carbon |
| $^oC$ | Degree Centigrade |
| cm | centimeter(s) |
| DOE | Designed Experiments |
| Dp | Particle Diameter |
| EDS | Energy Dispersive X-ray Spectroscopy |
| FIB | Focused Ion Beam |
| He | Helium |
| in | inch(es) |
| mm | millimeters |
| Mo | Molybdenum |
| Pt | Platinum |
| RTG | Radioisotope Thermoelectric Generator |
| Sb | Antimony |
| Se | Selenium |
| SEM | Scanning Electron Microscopy |
| SLPM | Standard Liters Per Minute |
| SNL | Sandia National Laboratories |
| Tp | Particle Temperature |
| Te | Tellurium |
| Vp | Particle Velocity |
| µm | micron |
| µΩ cm | micro-ohms-centimeter (unit for electrical resistivity) |
| Ω | Ohm (unit for electrical resistance) |
| Ω/sqr | Ohms per square (unit for sheet resistance) |

# 1. INTRODUCTION

Small (~100µm wide x ~500µm long) molybdenum (Mo) interconnects are needed to fabricate bismuth-telluride ($Bi_2Te_3$) based thermoelectric modules. Experiments were conducted in May – August 2013 to evaluate the feasibility of preparing these interconnects using the Air Plasma Spray (APS) process. Bismuth Telluride melts at 585°C [1] whereas Molybdenum melts at 2623°C [2]. Air Plasma Spray is a droplet deposition process in which a powder feed stock material is melted and propelled toward a substrate. When the feed stock droplets impact the substrate, they deform, solidify, and build a coating [3]. Air plasma spray torches can effectively work high melting point materials such as molybdenum because they use an extremely high temperature (~ 10,000°C) inert gas plasma as the heat source.

Molybdenum is a common APS coating. Molybdenum coatings are used commercially in conjunction with other materials as bond coatings because they exhibit very high adhesion strengths on steel substrates. Molybdenum coatings are also used to provide resistance wear and electric arc erosion. Plasma sprayed Mo coatings are used in air at service temperatures up to 315°C (600°F) [4].

The main goal of this project is to produce patterned Mo interconnects on a Bi-Te thermoelectric stacks using air plasma spray. In order to achieve this goal, the project was broken down into three different phases:

**Phase I – Masking and APS Feasibility Demonstration**

This first phase of the project focused on answering three primary questions:

- Can an air plasma sprayed Molybdenum coating be expected to have adequate electrical conductivity for a thermoelectric application? This was a concern because thermal spraying in air can introduce oxide into the coating, which will subsequently reduce its electrical conductivity.
- Will air plasma sprayed Molybdenum adhere to a Bi-Te substrate without damaging the coating-substrate interface? This was a concern because no adhesion data existed for Molybdenum on Bismuth-Telluride.
- Can Molybdenum be sprayed through a mask to achieve the feature size needed for this thermoelectric application? This was a concern because molybdenum is a high heat capacity material and was expected to damage any masking material in its path.

**Phase II – APS Molybdenum Process Optimization**

In Phase II, a Designed Experiment (DOE) was conducted to determine the effect of plasma arc current, total plasma gas flow, and standoff distance on coating resistivity. This data was used to optimize spray conditions for low electrical resistivity. The optimized spray conditions were then used to produce Mo coatings on P-and N-types Bi-Te coupons and the coating/substrate interface was examined.

**Phase III – Demonstration of APS Mo on Thermoelectric Modules**

The final phase of the project involved a second DOE to further refine the molybdenum process conditions for lower electrical resistivity. Low resistivity Mo coatings on full scale thermoelectric module were produced. Subsequently, circuit testing was performed.

# 2. EXPERIMENTAL PROCEDURES

## 2.1. Molybdenum Coating Preparation

Just as many different welding processes exist (e.g. laser welding, electron beam welding, and shielded metal arc welding), many different thermal spray processes exist. All coatings discussed in this report were prepared using the Air Plasma Spray (APS) process. The APS process melts and propels feed stock using an inert gas plasma [3]. Air plasma spray torches can effectively work high melting point and high heat capacity materials such as Molybdenum. All Molybdenum coatings in this work were prepared using the TriplexPro®-210 air plasma spray torch (Sulzer-Metco, Inc. Westbury, NY) as shown in Figure 1. A schematic showing the interior design and operating principal of the TriplexPro®-210 torch is shown in Figure 2. The torch was mounted on an ABB IRB-6600 six axis robot, which controlled the spray path. Three commercially available Molybdenum feed stock powders optimized for thermal spray were used.

**Figure 1: TriplexPro®-210 air plasma spray torch (Sulzer-Metco, Inc. Westbury, NY) used to prepare molybdenum coatings at Sandia's Thermal Spray Research Laboratory.**

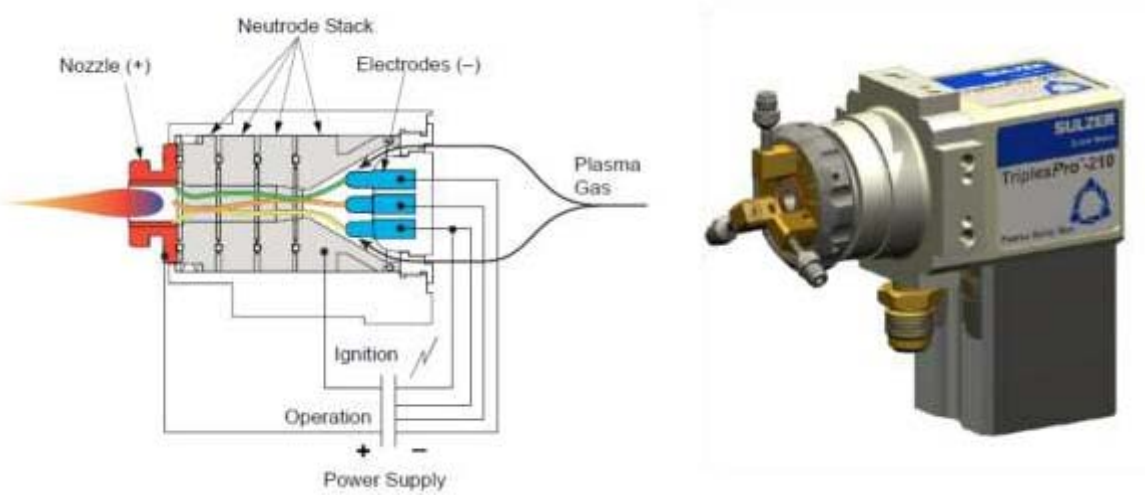


**Figure 2: Schematic (left) and image (right) of a TriplexPro®-210 air plasma spray torch. The three cathode extended arc design of the Triplex provides an extremely stable high energy plasma that can effectively spray a wide range of materials. [5].**

The primary difference between the three Mo powders was their mean particle size (~70 μm, ~30 μm, and ~10 μm) and particle size distribution. A variety of torch operating conditions were used to prepare molybdenum coatings during this development process. Exact torch operating conditions and powder specifications are provided in tables throughout the report as each coating and/or designed experiment is discussed.

## 2.2. Mask Preparation

Successfully masking the coating is critical to this application. The masks used contain feature sizes, geometries, and patterns representative of the features needed for the thermoelectric module application. The mask design is shown in Figure 3. Three types of Kapton masks were cut using an EDI 150W $CO_2$ laser cutter. The first group of masks was cut from clean Kapton sheet. The second group of masks were cut from Kapton sheet and coated by Au (Figure 4). Finally, the third group of masks was cut from carbon-filled Kapton tape (~0.003" thick with adhesive on the back side) as shown in Figure 5. DuPont's recommended operating temperature range for Kapton tape is -269$^{o}$C to 400$^{o}$C. The carbon-filled Kapton tape (DuPont Kapton HN) was stuck to a piece of Mylar prior to cutting. The laser cutter settings used were: pulse period of 9000 μs, pulse spacing of 30 μs, feed rate of 0.080 in/sec, and air pressure of 5 PSI. Prior to spray coating, the masks were inspected using an optical stereoscope. Figure 5 showed that the as-cut masks on Kapton tape were not completely clean. Small pieces of Mylar stuck to the openings in the pattern, leading to rough edges. These unwanted pieces are expected to degrade the integrity in the coating's features, as well as edge and spacing retention.

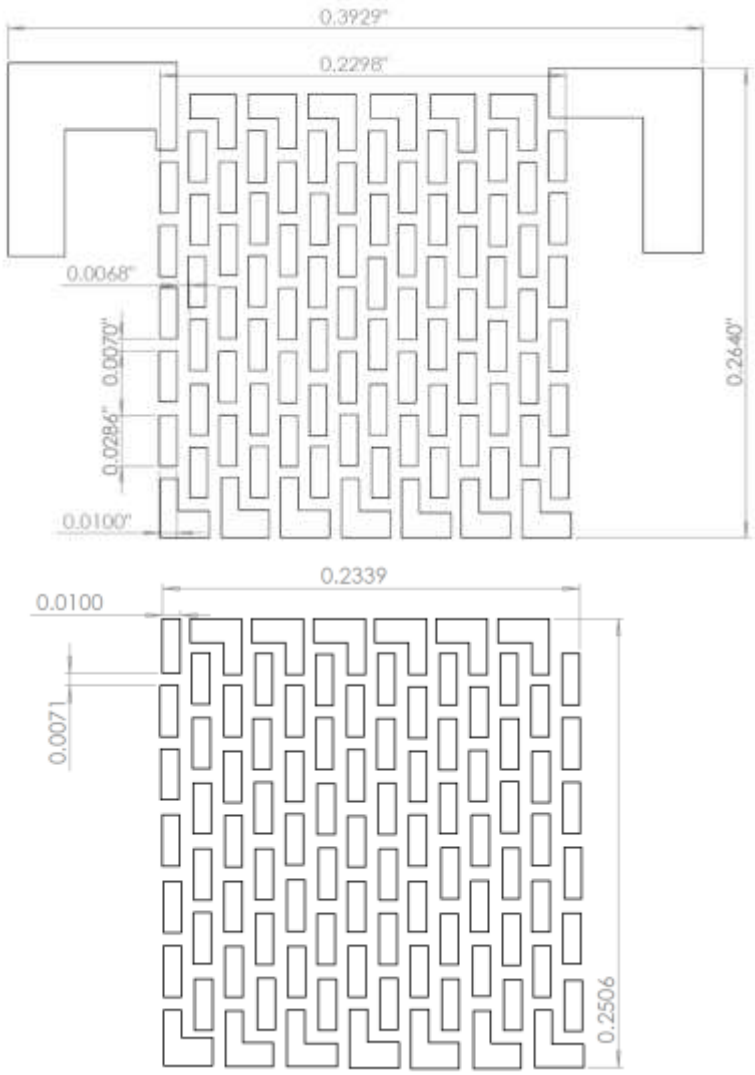


**Figure 3: Mask Design with dimensions. The two designs were used for opposite ends of the thermoelectric stack.**

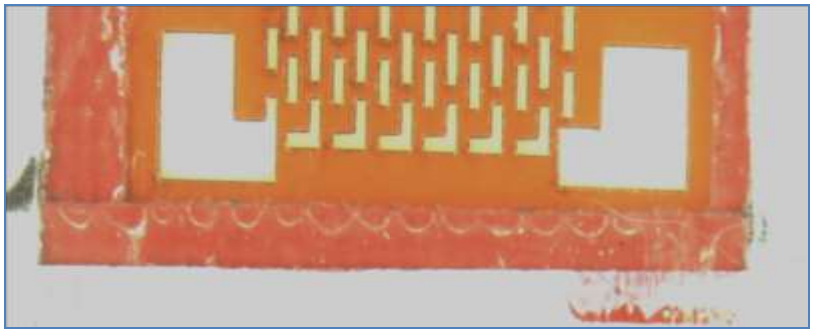

**Figure 4: An edge of the mask cut from Kapton sheet prior to spraying. The mask is surrounded by silicone tape (red material) and aluminum tape (white material) used to secure it during spraying.**

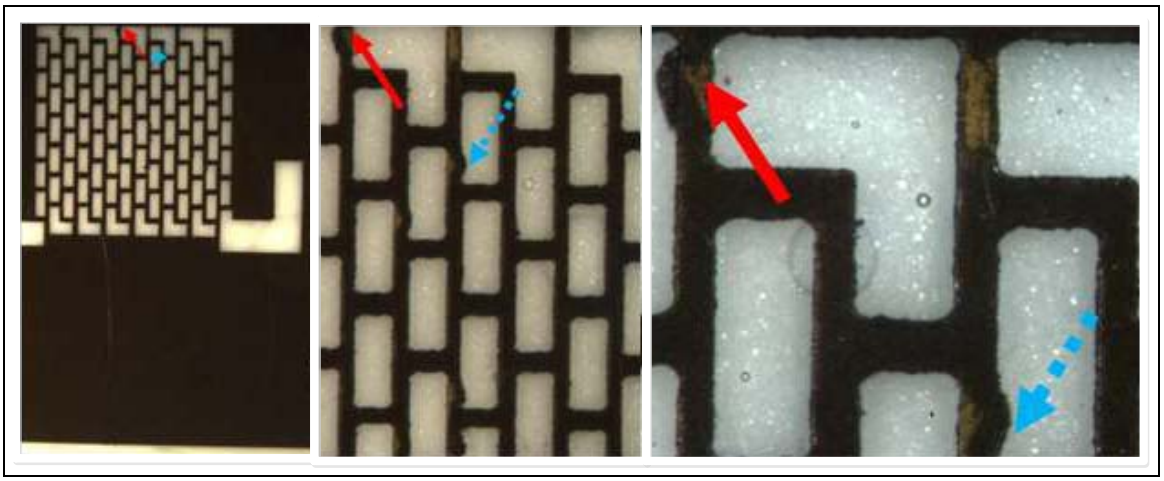

**Figure 5: As-received laser-cut mask prepared using carbon-filled Kapton tape on Mylar. The Kapton tape contains Carbon, providing the brown color to the tape. Note the disrupted edges (shown by arrows) on the mask already existed prior to spraying. Due to the line-of-sight nature of the thermal spray process, these non-uniformities in the mask will likely lead to a coating with poor feature edge retention and spacing.**

The masks cut from clean Kapton sheet and Au-coated Kapton sheet were attached to the substrates using silicone tape, applied at the edges of the mask (Figure 6). The masks cut from the carbon-filled Kapton tape were removed from the Mylar and carefully pressed onto the substrate. Silicone masking tape was applied manually around each Kapton mask. Finally, Aluminum tape was used to cover the remaining portion of the substrate prior to spraying. The masked substrate was attached to a rotary fixture for spraying, as shown in Figure 7. A rotary fixture was chosen for this coating application because it enabled substrate temperature management. As the torch traverses vertically across the rotating fixture, the masked component passes through the plasma plume and then immediately through a cooling air jet produced by an air knife positioned at ~ 90 degrees around the rotary fixture from the spray torch. All thermal spray tapes and masks were removed after spraying.

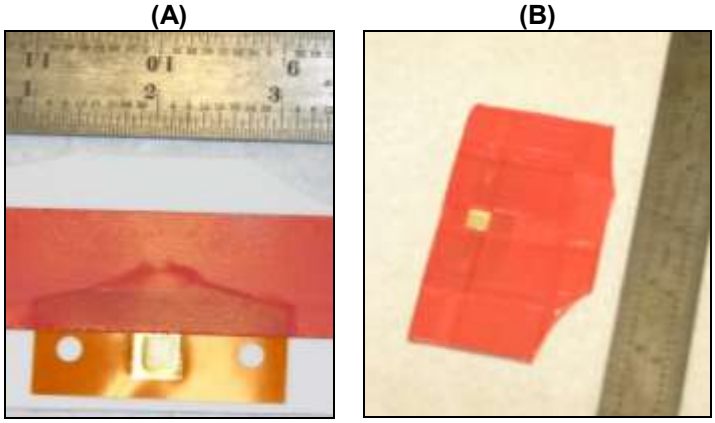


**Figure 6: A) Au-coated Kapton mask partially attached to an $Al_2O_3$ substrate with silicone tape. The Au coating was expected to protect the Kapton mask from the Molybdenum droplets. B) Fully masked and taped substrate prior to coating. Only the patterned area of the Kapton mask is exposed to the Molybdenum droplet stream.**

**Figure 7: Fully masked $Al_2O_3$ substrate (with silicone and aluminum tapes) attached to a rotary fixture ready to be plasma sprayed with Molybdenum. The air knife seen in the left foreground of this image is positioned ~90° from the spray plume. This allowed the coated part to rapidly pass through the plasma and then immediately through the cooling air jet as the fixture rotated.**

## 2.3. Electrical Resistivity Measurement

Four-point-probe measurements were performed on the sprayed Molybdenum coatings to characterize their electrical resistivity. Sheet resistance was measured using a Jandel cylindrical probe head which contained a linear four point probe array with a probe-to-probe spacing of 1mm. This probe head was attached to a Keithley 2400 source meter. Local sheet resistance was measured using the four-point-probe method by placing probes at several locations on the coating. Global sheet resistance was measured using the Van der Pauw method by placing probes at the edges of the coated surface [6]. Both local and global sheet resistance values were measured due to the non-uniform coating thickness, as well as the varying amount of voids, oxides, and porosity in the coating.

Sheet resistance is not an intrinsic material value because it contains coating thickness. To convert sheet resistance to electrical resistivity, the coating thickness value is needed. The film thickness (step height) was determined using a Dektak surface profilometer. Electrical resistivity was calculated by multiplying the reported global sheet resistance value to the average film thickness. Finally, the resistivity value of the sprayed Mo coating was compared to that reported for a bulk Mo sample of 5.5 $\mu\Omega$ cm [7]. It is expected that a large amount of porosity and oxide will exist in the thermal sprayed Mo films, leading to a much higher resistivity than that of the bulk Mo sample.

## 2.4. Microstructural Examination

Microstructural examination focused on the coating/substrate interface. Chemical interaction between the Mo droplets and the bismuth-telluride substrates was of key concern. Splat boundaries and solidification structure within the Mo droplets were also examined.

An FEI Helios dual platform focused ion beam (FIB) tool, equipped with both a $Ga^+$ ion column and a scanning electron microscope column, was used to produce cross sections of the sample normal to the deposition surface for both SEM imaging and energy dispersive x-ray spectrometry (EDS). Localized Platinum deposition was used to protect the surface of the sample from direct ion beam irradiation. Trenches were milled normal to the deposition surface. Subsequently, EDS was used to perform X-ray micro-analysis, delineating regions that were Mo rich, Bi/Te rich, and Pt rich. From this analysis, the coating/substrate interaction or lack thereof can be determined.

Metallographic cross-sections were performed using standard mounting and polishing techniques.

## 2.5. Particle Temperature, Velocity, and Diameter Measurement

Molybdenum particle temperature ($T_p$), particle velocity ($V_p$), and particle diameters ($D_p$) were measured in-flight, using a DPV-2000 (Tecnar Automation Ltd., St.-Bruno, QC, Canada), particle diagnostic system. This system was used by positioning the centerline of the plasma spray plume in front of the DPV-2000's optical sensor at the set standoff distance. The DPV-2000 measures individual particle properties using a unique optical system. Particle temperature measurements are made using two-color pyrometry. Optical emissions from individual particle are captured at wavelength bands of $\lambda_1$= 787±25nm and $\lambda_2$= 995±25nm. Particle temperature at these wavelengths is determined by spectral radiation density of a blackbody (Wien's approximation of Planck's law) assuming gray-body emissivity $\varepsilon(\lambda_1)/\ \varepsilon(\lambda_2)=1$[8]. Individual particle velocities are determined by measuring each particle time-of-flight as it crosses the DPV-2000's measurement volume. Individual particle diameters are estimated from the amount of the sensor field of view obscured as the particle transits the DPV-2000's measurement volume. Sophisticated particle detection algorithms allow correlation of individual particle temperature, velocity, and diameter measurements.

# 3. PHASE I - FEASIBILITY DEMONSTRATION

This first phase of this project consisted of three primary feasibility demonstrations, preparation of conductive molybdenum coatings, adhesion of molybdenum to bismuth-telluride, and masking of APS Mo coatings to produce a high resolution pattern. The masking demonstration is discussed first.

## 3.1. Masking Feasibility

It was expected that the high temperature Mo spray plume would destroy the masks. However, the mask was not destroyed. Two spray conditions were used to prepare Molybdenum coatings. The conditions shown in Table 1 were used to evaluate all three Kapton masks, by spraying Mo through the mask, onto a flat $Al_2O_3$ substrate. The conditions shown in Table 1, Set Point 1 were used to spray through masks cut from clean Kapton sheet and Au-coated Kapton sheet. The conditions in Table 1, Set Point 2 were used to spray through masks cut from carbon-filled Kapton tape. Both conditions in Table 1 were used to coat bismuth-telluride substrates for metallographic examination.

The masks cut from Kapton sheet with and without Au-coating as well as those cut from the Kapton tape were virtually undamaged by the plasma sprayed Molybdenum as shown in Figure 8, Figure 9 and Figure 10, respectively. The only damage noted was damage to the sputtered Au layer on the surface of the mask in Figure 8. The Au coating was present because the masks had already been used for Au-sputtering experiments. Au coating is not a necessary part of the mask, is not needed, and did not provide a benefit as originally expected. Because such extensive damage was observed in the sputtered Au coating, a second sample was sprayed using a mask that was not Au-coated, as shown in Figure 9. Similarly, no significant damage to the Kapton mask was observed. Specifically, the edges of the mask features remained intact and the Kapton has not been damaged other than minor pock marking of its surface by the liquid Mo droplets. Likewise, the masks cut from Kapton tape were not damaged, as shown in Figure 10.

**Table 1: Process parameters and set points used to prepare Molybdenum coatings for initial mask evaluation. Masks cut from clean Kapton sheet (Set Point 1), Au-coated Kapton sheet (Set Point 1), and carbon filled Kapton tape (Set Point 2) were placed on $Al_2O_3$ substrates and coated using these conditions. The same parameters were also used to prepare coatings onto bismuth-telluride substrates for metallographic examination.**

| Process Parameter | Set Point 1 | Set Point 2 |
|---|---|---|
| **Spray Torch** | **TriplexPro®-210** | **TriplexPro®-210** |
| Current | 520 A | 520 A |
| Argon | 35 SLPM | 35 SLPM |
| Helium | 20 SLPM | 20 SLPM |
| Nozzle | 9mm | 9mm |
| Powder Injector | 1.8mm | 1.8mm |
| Injector Holder | 90L | 90L |
| Injector Holder Offset | 20° | 20° |
| | | |
| **Powder Hopper** | **Sulzer-Metco 9MP-CL** | **Sulzer-Metco 9MP-CL** |
| Powder Gas Flow (Argon) | 4 SLPM | 4 SLPM |
| Powder Hopper pressure | 200 mbar | 200 mbar |
| Pneumatic Vibration pressure | 2000 mbar | 2000 mbar |
| Powder Feed Rate | 10 g/min | 10 g/min |
| Air Jet Cooling pressure | 4 Bar | 4 Bar |
| | | |
| **Spray Pattern** | **7$^{th}$ Axis: Spindle** | **7$^{th}$ Axis: Spindle** |
| Stand Off Distance | 10 in | 10 in |
| Number of passes | Varies by sample | Varies by sample |
| Effective Traverse speed | 800 mm/s | 800 mm/s |
| Rotation Velocity | 602 deg/s | 602 deg/s |
| Linearly Velocity | 50.7 mm/s | 50.7 mm/s |
| | | |
| **Powder** | **Bay State Abrasives 70 μm Mo** | **Bay State Abrasives 10 μm Mo** |
| Particle Size | 67.43μm ± 9.58μm | 10.88μm ± 9.17μm |
| Powder Morphology | Spherical Gas Atomized | Spherical Gas Atomized |

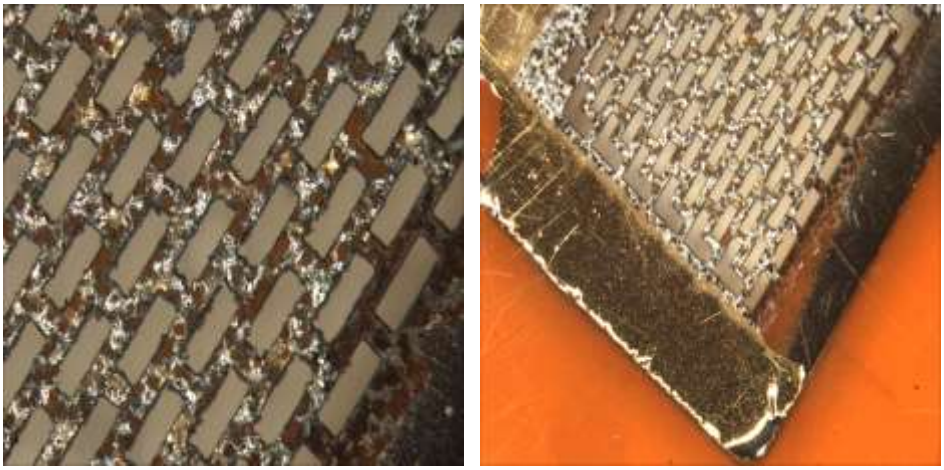

**Figure 8: Two images of the Au coated Kapton mask after spraying with 8 passes of Mo (~70 µm size powder). The Mo droplets melted the Au sputter coating, causing the Au coating to delaminate from the Kapton substrate. No damage to the Kapton edges or the Kapton itself is observed on this mask.**

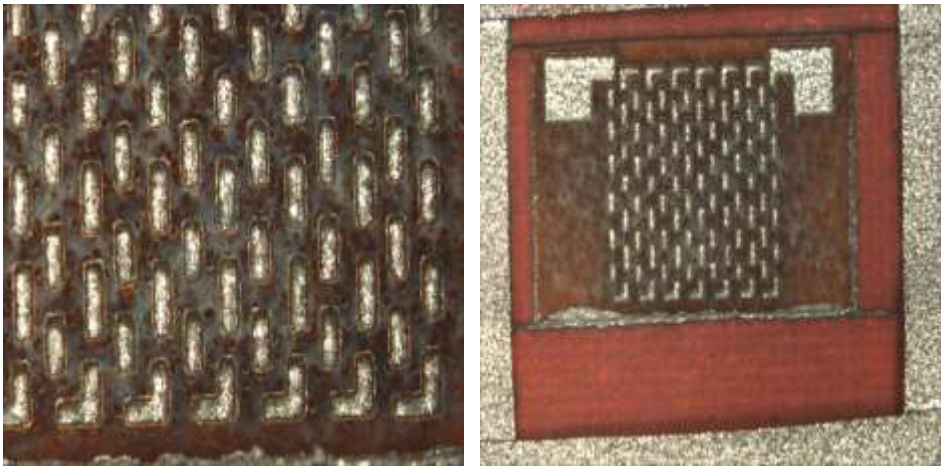

**Figure 9: Two images showing masks cut from Kapton sheet without Au coating after spraying with 24 passes of Mo (~70 µm size powder). No significant damage to the mask is observed. Mo droplets left pock marks on the mask surface but they have not burned the mask or caused loss of edges or features. The Mo coating can clearly be seen beneath the mask.**

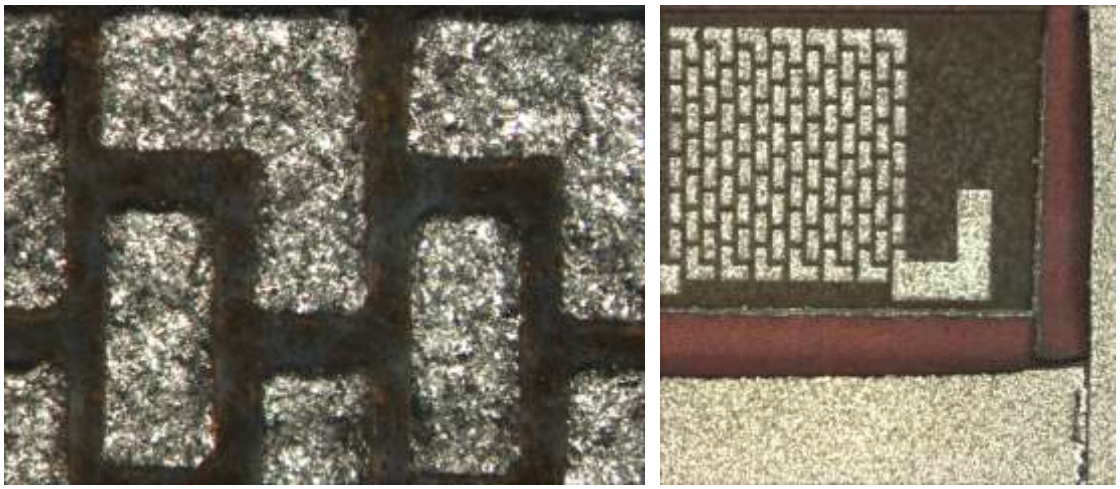

**Figure 10: Two images of the masks cut from carbon filled Kapton tape after spraying with Mo (~10 µm size powder). No damage to the Kapton edges or the Kapton itself is apparent on this mask.**

### *3.1.1. Coating Edge and Feature Retention*

Initial coating tests proved that Kapton masks can survive the Molybdenum plasma spray coating process. However, the Molybdenum patterns created using the masks cut from the Kapton sheet were not good quality (Table 1, Set Point 1). As shown in Figure 11, edge and feature retention are poor. Feature retention was poor because the masks cut from Kapton sheet were simply held in place over the substrate with tape. This resulted in a small gap between the mask and the substrate because there was no adhesive on the underside of the Kapton. As a result, the Mo droplets splashed beneath the mask and resulted in Mo deposition under the mask, leading to poor edge retention.

Fortunately, the edge retention problem was addressed by using a smaller Mo powder (Table 1, Set Point 2) and a thinner mask (0.003” or ~58µm instead of 0.006”) which was cut from Kapton tape. The problem of deposition beneath the mask was eliminated using this approach. Figure 12 shows a Molybdenum coating prepared using the ~10µm powder and the mask cut from Kapton tape. Notice that the coating has excellent edge and feature retention (~170µm).

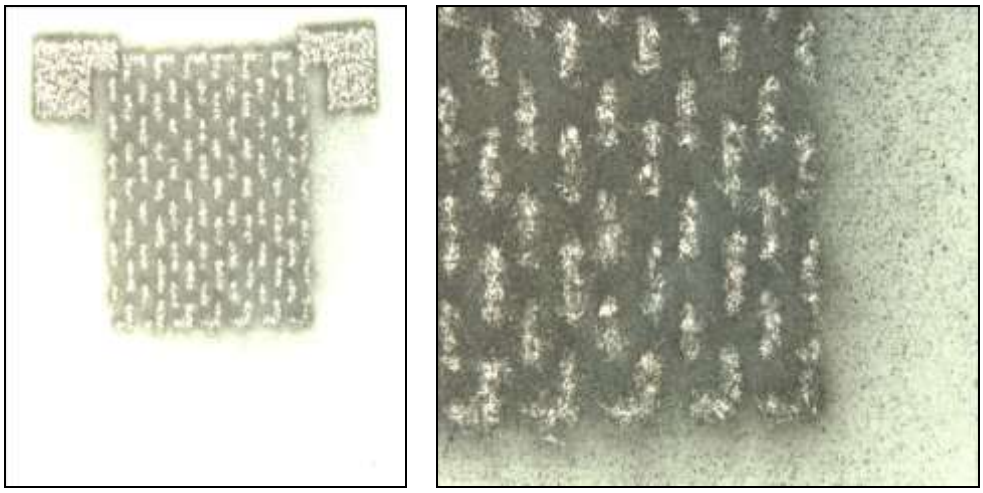

**Figure 11: Initial attempt at preparing a patterned Mo coating (8 passes) on an $Al_2O_3$ substrate resulted in poor edge and feature retention. Splashing of Mo beneath the mask can be seen. This splashing and the large Mo particle size used (~70 µm) contributed to poor feature definition.**

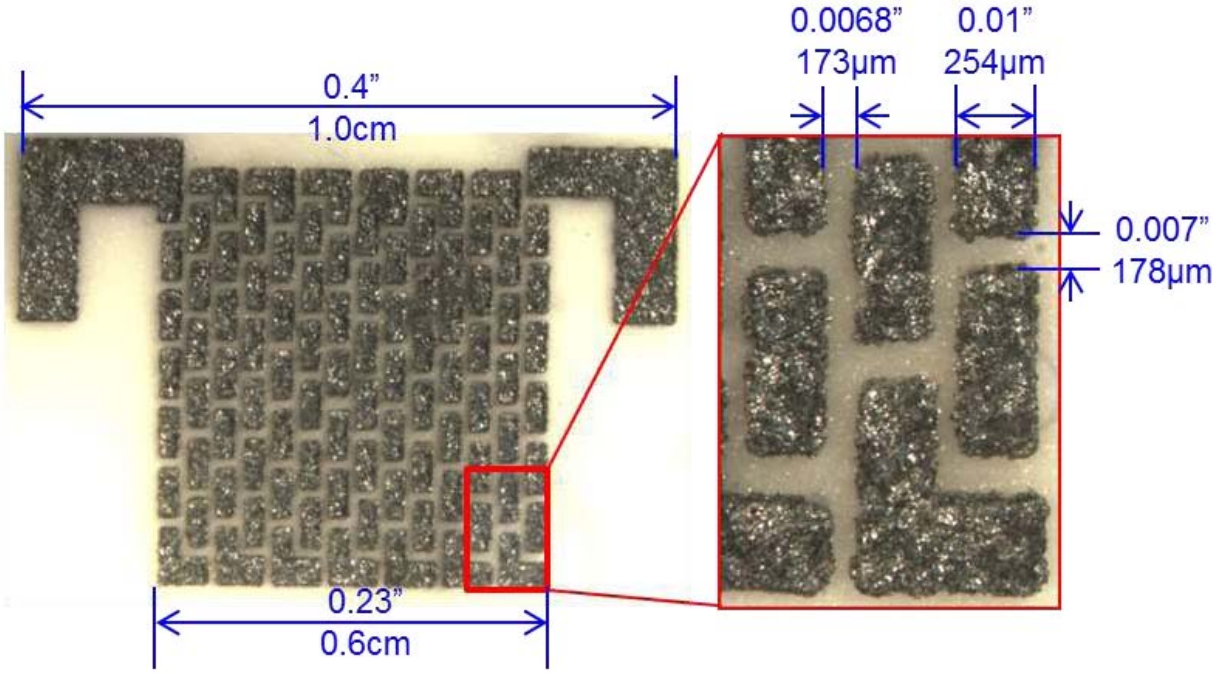


**Figure 12: Improved Mo coating (~10µm powder, 20 passes) on an $Al_2O_3$ substrate with reduced splashing and excellent feature definition. Some missing edges due to residue on the laser-cut Kapton tape masks were occasionally observed.**

A number of important lessons were learned developing this coating and masking process. First, the as-cut masks on Kapton tape had rough edges because there were adhesive and Mylar residues in the openings of the pattern. These unwanted residues obstructed the particle path to

the substrate and degraded the integrity of the coating's edge and feature definition. The best coating results were obtained by carefully following these steps:

1. Clean the as-received laser-cut mask Kapton tape by gently rubbing the surface of the mask using TX4004 synthetic wipers (MiracleWipe®) and soapy water.
2. After removing the mylar layer from the back of the Kapton tape, apply the Kapton tape to the substrate immediately. Use a hard edge to press down and rub the Kapton tape mask gently to remove any air bubbles.
3. Perform the spray process within 2 hours after properly attaching the Kapton tape to the substrate.
4. After the spray process, gently peel-off the Kapton tape.

## 3.2. Coating Electrical Properties

Four-point-probe measurements were performed on sprayed Molybdenum coatings to determine electrical resistivity and thus the feasibility of this coating as interconnect. Local sheet resistance was determined to be between 0.05 - 0.6 ohms/square. The order of magnitude difference in the local sheet resistance was likely due to the non-uniform coating thickness as well as the varying amount of voids, oxides, and porosity in the coating. Global sheet resistance, as determined by placing probes at the edges of the coated surface, was measured as 0.520 Ω/square.

Sheet resistance is not an intrinsic material property because it is dependent on thickness. The film thickness was ~5.8 μm (in step height). This thickness value may not be entirely accurate due to the non-uniform and rough nature of the thermally sprayed coating. Nonetheless, the electrical resistivity was calculated using the reported global sheet resistance value of 0.520 Ω/square and the average thickness of ~5.8 μm. The sprayed Mo coating has a resistivity of 301.6 μΩ cm. This resistivity value is higher in comparison to that reported for bulk Mo: 5.5 μΩ cm [6]. We expect that a large amount of porosity and oxide in the thermal sprayed Mo film is responsible for its low conductivity.

## 3.3. Coating Microstructure

Coating microstructure was examined using Scanning Electron Microscopy (SEM) with Energy Dispersive Spectroscopy (EDS). In addition, metallographic cross-sections and Focused Ion Beam (FIB) cross-section with EDS were utilized for examining the solidification mode of the Mo coating as well as the Mo/$Bi_2Te_3$ interface. The overall results showed that the coating exhibited excellent edge and feature retention and no coating/substrate interaction was observed.

SEM images of the sprayed Mo coating (10μm powder size, 4 passes) on $Bi_2Te_3$ substrate showed that the coating conformed to the features cut into the Kapton tape mask as seen in Figure 13. Figure 13 also showed that both the $Bi_2Te_3$ substrate and the Mo coating are very rough and non-uniform. The Mo coating on this sample is thin. Thicker Mo deposits can be seen around the edges of the feature (the mask edge) than in the middle of the feature. Higher magnification of SEM images (Figure 14) revealed small particulate-like features on top of the Mo splats. These features suggested that some of the Mo powders were vaporized during the spray process and re-condensed onto the existing Mo splats.

Figure 15 showed EDS maps of the Mo coating surface. The coating is thin and non-uniform. Both Mo coated regions and exposed substrate can be seen, as evidenced by the Bi, Te, and Se maps in Figure 15. Se was identified as a dopant in the n-type Bi-Te substrates.

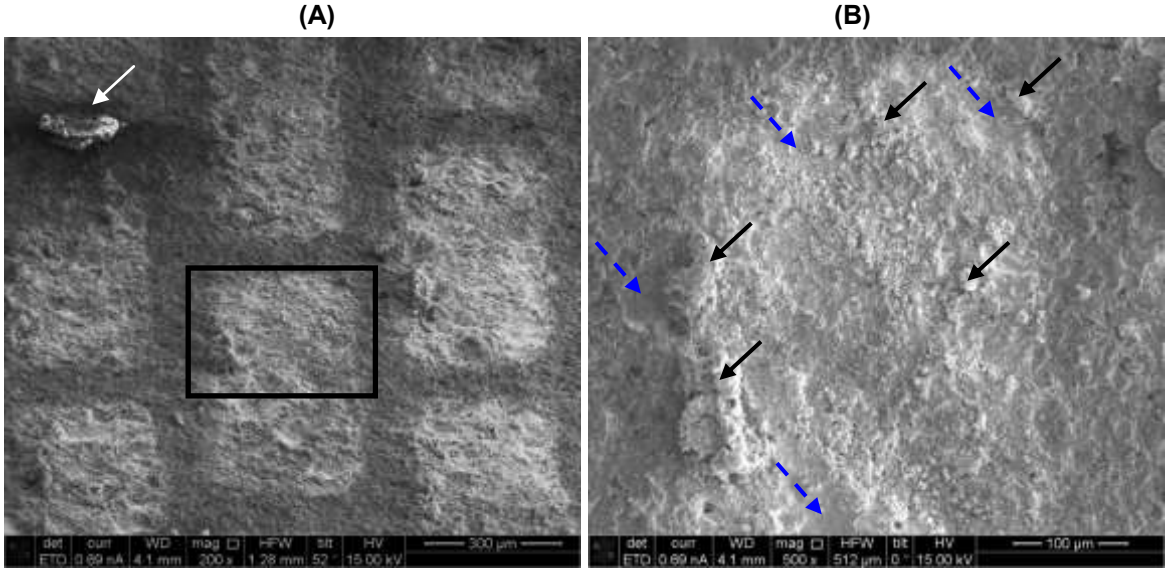


**Figure 13: Mo coating (10µm powder size, 4 passes) on $Bi_2Te_3$ substrate. A) SEM image showing the Mo coated areas (light rectangular regions) and the substrate (dark areas). The coating appears rough and non-uniform. Adhesive residue is marked with the white arrow. B) High magnification SEM image showing a Mo coated region. Molybdenum splats (dotted blue arrows) and larger Mo particles (solid black arrows) were observed.**

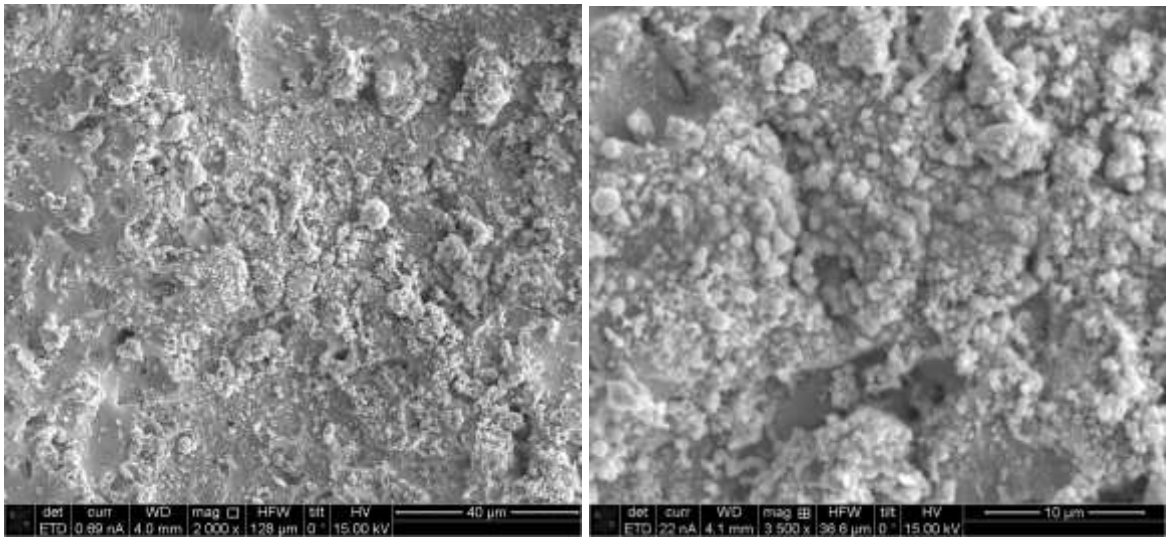

**Figure 14: High magnification SEM images showing the Mo coating (10µm powder size, 4 passes) on $Bi_2Te_3$ substrate.**

Figure 16 shows FIB cross sections of the Mo coating. Dendritic solidification in the molten Mo droplets is clearly visible, (Figure 16 C-F). This suggests that Mo feedstock powder is not 100% pure because dendritic solidification involves solute rejection from the dendrites which results in solute-enriched regions between the dendrite arms after solidification is completed. This is not

unexpected when using a commercially pure Mo powder. Pores were observed at the Mo splat boundaries, at the coating/substrate boundaries, and within the splats. In addition, pores and grain boundary cracks were observed deep within the substrate. FIB/EDS analysis (Figure 17) showed a clear distinction between the Mo coating and the Bi, Te, and Se substrate. These data show that no chemical interaction (alloying) between the coating and substrate has occurred.

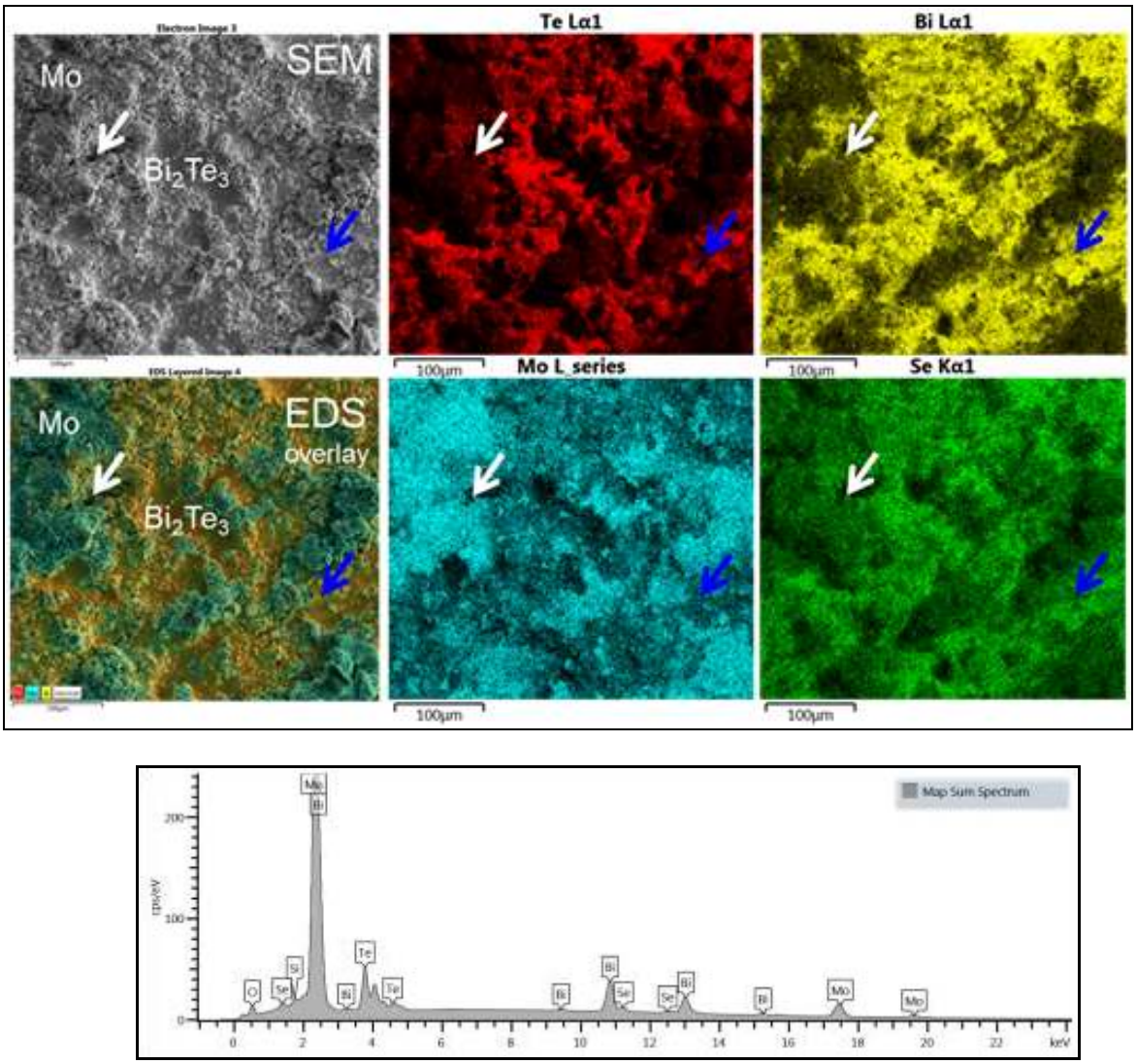


**Figure 15: EDS maps showing the Mo coating surface. Bi (yellow), Te (red), and Se (green) are present in the substrate. Mo (cyan) is present in the coating. The arrows in the figures point to the same features.**

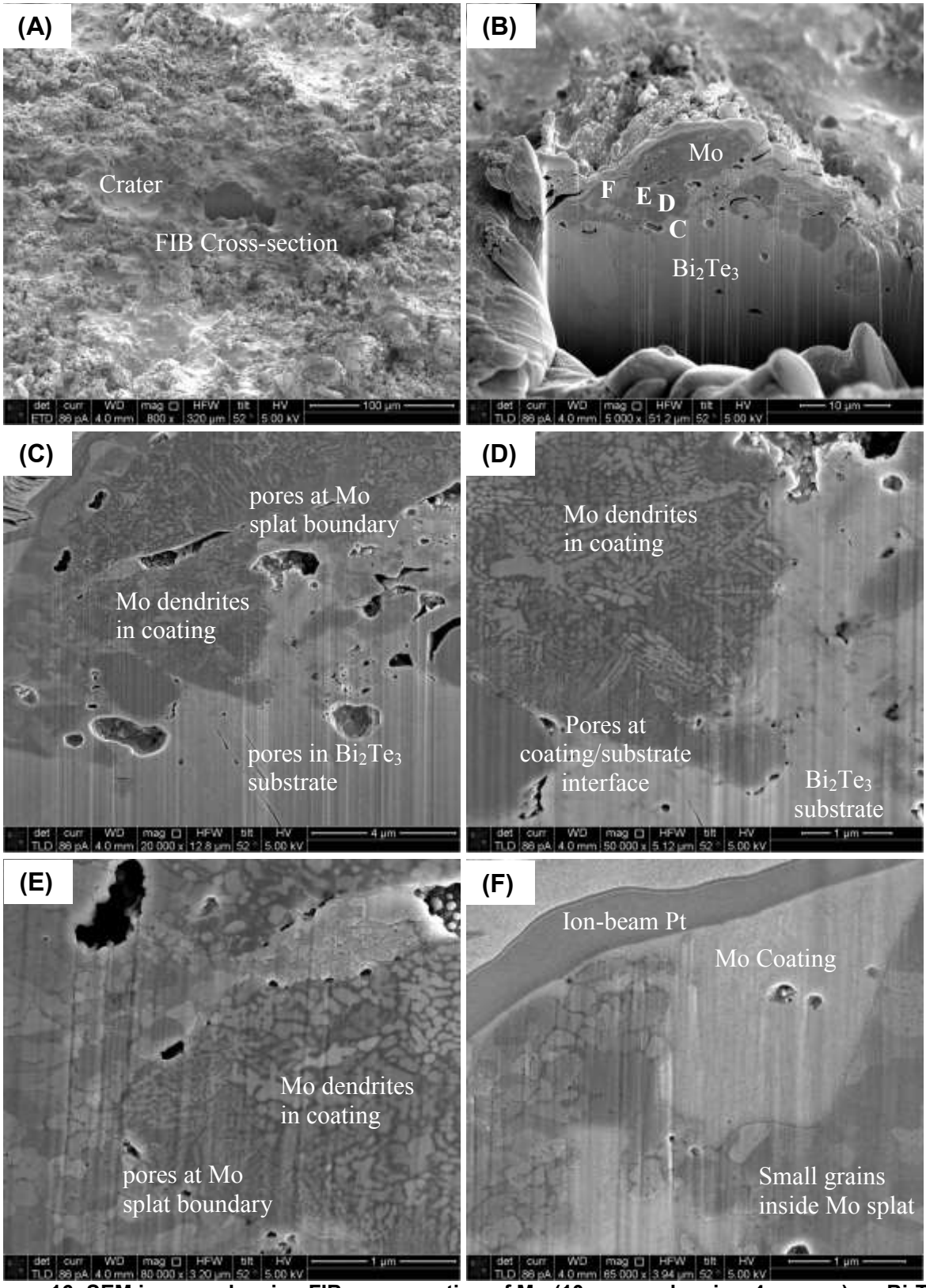


**Figure 16: SEM images showing FIB cross-section of Mo (10µm powder size, 4 passes) on $Bi_2Te_3$ (A), revealing pores in the substrate (B,C), at the coating/substrate interface (C,D), and at splat boundaries within the coating (E,F). Mo coating exhibited dendritic solidification (C-F).**

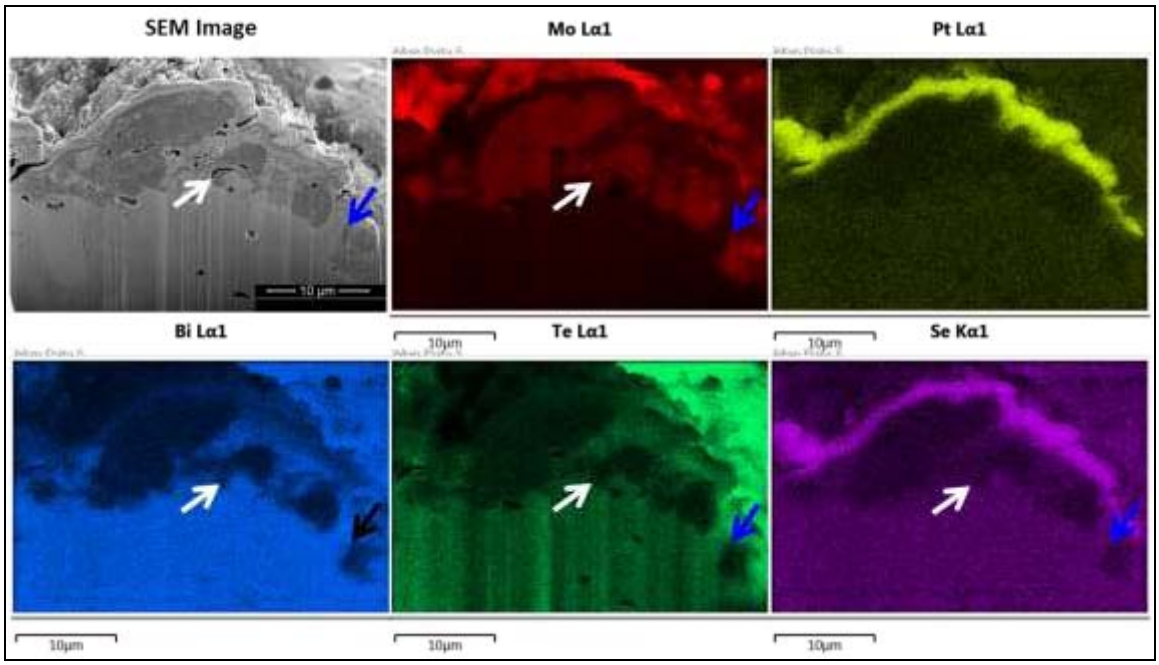


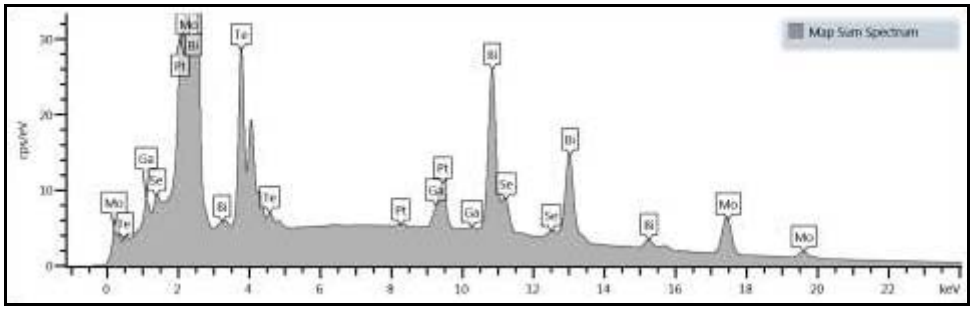


**Figure 17: EDS analysis of the Mo coating cross section (10µm powder size, 4 passes). Distinct regions can be seen including: the Pt protective layer on the coating surface, the Mo coating, as well as Bi and Te (and Se) in the $Bi_2Te_3$ substrate. No significant Mo/$Bi_2Te_3$ mixing was observed at the interface.**

In addition, to the FIB cross-sections above, metallographic cross-sections were prepared from the 70µm powder size Mo coating. A metallographic cross-section of the uncoated Bi-Te substrate is shown in Figure 18. Cracks and voids can be seen at the top surface as well as in the bulk bismuth-telluride sample. Cross-sections through the coating and substrate are shown Figure 19, Figure 20, and Figure 21. Pronounced cracks can be seen underneath the coatings. Voids are also observed at the coating/substrate interface and in the coating itself. Micro-voids and micro-cracks were also observed between the coating splat boundaries as shown in Figure 21. We suspect that these cracks are formed by stress fields created by the voids. We also suspect that the voids are formed by Tellurium vaporization due to local heating by the solidifying Mo droplets. We expect that decreasing the Mo particle size, optimizing the spray condition to reduce Mo particle temperature, and introducing more aggressive substrate cooling will alleviate the substrate cracking and vaporization issues. This has not yet been demonstrated.

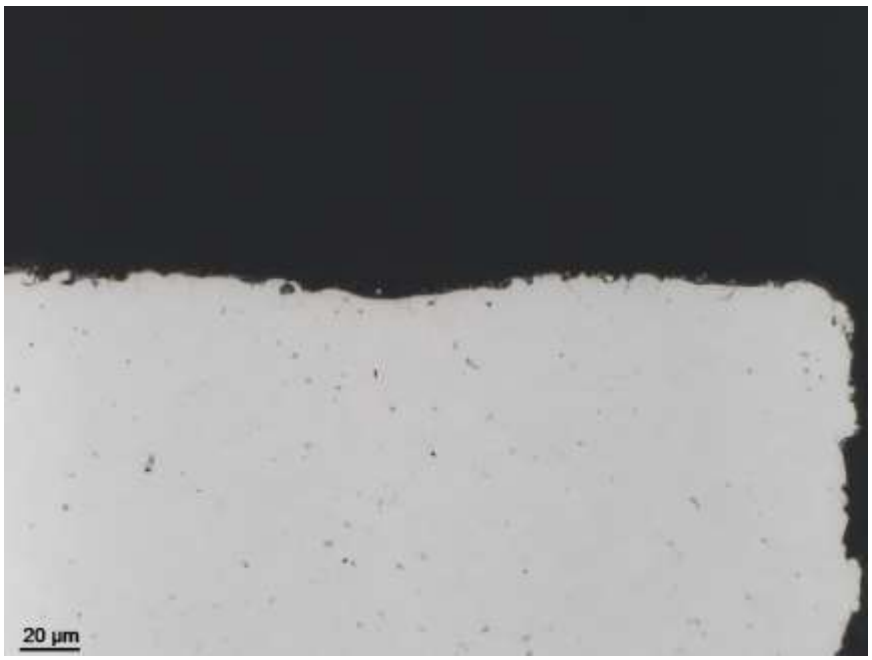


**Figure 18: Polished cross section of the unsprayed $Bi_2Te_3$ substrate. This higher magnification picture still showed signs of pre-existing voids and cracks right below the substrate surface, along the grain boundaries.**

**Figure 19: Polished cross section of the sprayed Mo (70µm powder size) on $Bi_2Te_3$ substrate. The coating/substrate interface appeared wavy and contained voids. Note that cracks are present immediately below the coating-substrate interface, along the grain boundaries the $Bi_2Te_3$.**

**Figure 20: Polished cross section showing the Mo (70µm powder size) coating on the $Bi_2Te_3$ substrate. The transition between the sprayed and masked regions can be seen at the right side of the image. Notice that the uncoated substrate on the right-hand side is much smoother (more planar) compared to the substrate beneath the Mo sprayed coating on the left-hand side of the image.**

**Figure 21: Polished cross section showing sprayed Mo (70µm powder size) coating on the $Bi_2Te_3$ substrate. This higher magnification image showed signs of possible Mo-$Bi_2Te_3$ mechanical interaction at the wavy coating/substrate interface. Subsequent layers of Mo showed the elongated grains "splats" containing columnar structures, typical of coatings prepared using APS. Note the cracks immediately below the interface, along the grain boundaries of the $Bi_2Te_3$ substrate.**

## 3.4. Phase I Feasibility Demonstration Summary

The best preliminary Air Plasma Sprayed (APS) Molybdenum coating was achieved using a 10µm sized powder and mask laser-cut from Carbon-filled Kapton tape. The coating had excellent feature and spacing retention (~170µm size), but exhibited some porosity at the splat boundaries and at the coating/substrate interface. Nevertheless, this feasibility study proved:

- Mo can be sprayed through a mask to achieve the feature size needed for this thermoelectric application.
- APS Mo coating prepared using a 10µm powder adheres to a $Bi_2Te_3$ substrate. Minimal Mo/ $Bi_2Te_3$ interaction at the coating substrate interface was observed.
- The initial APS Mo coating exhibits an electrical conductivity that is adequate for a thermoelectric application

Porosity at the coating substrate interface suggests Tellurium vaporization is the likely cause of substrate cracking. Importantly, analysis of the APS Mo coating did not reveal any significant chemical interaction between the Mo and the $Bi_2Te_3$ substrate at the coating/substrate interface. The coating's electrical conductivity was measured and shown to be 301.6 µΩ cm. This is adequate for this thermoelectric application but does not compare well to bulk Mo (5.5 µΩ cm). Tellurium vaporization, substrate cracking, and coating porosity leading to low electrical conductivity, can all be mitigated through APS process optimization. This process optimization was pursed in Phase II.

# 4. PHASE II - APS PROCESS OPTIMIZATION

The goal of Phase II is to optimize the APS process, to produce a Mo coating with the lowest resistivity value. This was achieved using a $3^2$ full factorial design of experiment (DOE). Three factors—arc current, total plasma gas flow and standoff distance—were varied over two levels. Because the Phase 1 coatings showed signs of Mo vaporization and re-deposition, the DOE was designed to decrease the Mo particle temperature and velocity. Thus, lower arc currents, lower plasma gas flows, and longer standoff distances were explored. The most optimal condition from the DOE was used to prepare Mo coatings on N-type and P-type Bi-Te substrates. The microstructure and electrical resistivity of the coating were examined.

## 4.1. Designed Experiment (DOE) for APS Mo Process Optimization

In this DOE, the factors (and their high/low points) were arc current (350A/450A), total plasma gas flow (60.5 SLPM / 110 SLPM), and standoff distance (152.4mm/254mm). The Ar:He gas ratio was arbitrarily fixed at 1.75:1. A full factorial design with 3 center points was selected as shown in Table 2. Other process parameters, held constant throughout the DOE are listed in Table 3. MiniTab® software was used to conduct all ANOVA analysis of the DOE data.

**Table 2: Full factorial design used for the Mo Phase II DOE. Arc Current, Total Plasma Gas Flow and Standoff Distance were varied. Argon Flow and He Flow were calculated using a fixed Ar:He ratio of 1.75:1.**

| Run Order | Center Pt | Blocks | *Arc Current (Amps) | *Total Plasma Gas Flow (SLPM) | *Standoff (mm) | Argon Flow (SLPM) | He Flow (SLPM) |
|---|---|---|---|---|---|---|---|
| 1 | 1 | 1 | 350 | 60.5 | 254 | 38.5 | 22 |
| 2 | 1 | 1 | 450 | 60.5 | 152.4 | 38.5 | 22 |
| 3 | 1 | 1 | 350 | 110 | 254 | 70 | 40 |
| 4 | 1 | 1 | 450 | 110 | 152.4 | 70 | 40 |
| 5 | 1 | 1 | 450 | 110 | 254 | 70 | 40 |
| 6 | 0 | 1 | 400 | 85.25 | 203.2 | 54.25 | 31 |
| 7 | 1 | 1 | 450 | 60.5 | 254 | 38.5 | 22 |
| 8 | 0 | 1 | 400 | 85.25 | 203.2 | 54.25 | 31 |
| 9 | 0 | 1 | 400 | 85.25 | 203.2 | 54.25 | 31 |
| 10 | 1 | 1 | 350 | 60.5 | 152.4 | 38.5 | 22 |
| 11 | 1 | 1 | 350 | 110 | 152.4 | 70 | 40 |

**Table 3: Process parameters and set points held constant throughout the Phase II DOE.**

| Process Parameter | Set Point |
|---|---|
| **Spray Torch** | **TriplexPro®-210** |
| Current | 350, 400 or 450 Amps |
| Argon | 38.5, 54.25, or 70 SLPM |
| Helium | 22, 31, or 40 SLPM |
| Nozzle | 9mm |
| Powder Injector | 1.8mm |
| Injector Holder | 90L |
| Injector Holder Offset | 20° |
| | |
| **Powder Hopper** | **Sulzer-Metco 9MP-CL** |
| Powder Gas Flow (Argon) | 5-8 SLPM |
| Powder Hopper pressure | 200 mbar |
| Pneumatic Vibration pressure | 2000 mbar |
| Powder Feed Rate | 10 g/min |
| Air Jet Cooling pressure | 4 Bar |
| | |
| **Spray Pattern** | **7$^{th}$ Axis: Spindle** |
| Stand Off Distance | 5, 7.5, or 10 in |
| Number of passes | 5 or 10 passes |
| Effective Traverse speed | 800 mm/s |
| Rotation Velocity | 602 deg/s |
| Linearly Velocity | 50.7 mm/s |
| | |
| **Powder** | **Mo-11 from Plasmadyne** |
| Particle Size | 36.378µm ± 10.933µm |
| Powder Morphology | Spherical Gas Atomized |

Molybdenum powder with a mean diameter of 36.378µm was used throughout this DOE. This choice was made because of limited Mo feed stock availability. Note: 10 µm Mo powder is available but must either be imported or must be custom made in the US, resulting in a long (~3month) lead times. Molybdenum coatings were prepared on $Al_2O_3$ substrates at each condition identified in Table 3.

Results from the DOE, detailing the Kapton tape survival, powder injection flow rate, particle velocity/temperature/diameter, and sheet resistance for all samples are shown in Table 4.

**Table 4: DOE Results: Vp, Tp, Dp, Kapton Survival, and Mo Sheet Resistance**

| Run Order | Center Pt | Blocks | *Arc Current (Amps) | *Total Plasma Gas Flow (SLPM) | *Standoff (mm) | Argon Flow (SLPM) | He Flow (SLPM) | Kapton Survive? | Powder Injection Flow (SLPM) | Vp Mean (m/s) | Tp Mean (deg C) | Dp Mean (µm) | Sheet Resistance (Ω/sqr) |
|---|---|---|---|---|---|---|---|---|---|---|---|---|---|
| 1 | 1 | 1 | 350 | 60.5 | 254 | 38.5 | 22 | Y | 5 | 194.994 | 2846.303 | 14.882 | 0.030351 |
| 2 | 1 | 1 | 450 | 60.5 | 152.4 | 38.5 | 22 | N | 5 | 292.588 | 2820.388 | 13.637 | 0.110532 |
| 3 | 1 | 1 | 350 | 110 | 254 | 70 | 40 | Y | 7 | 274.458 | 2847.126 | 14.283 | 0.042884 |
| 4 | 1 | 1 | 450 | 110 | 152.4 | 70 | 40 | N | 8 | 380.957 | 2816.62 | 15.468 | 1.387992 |
| 5 | 1 | 1 | 450 | 110 | 254 | 70 | 40 | Y | 8 | 315.379 | 2837.106 | 15.199 | 0.072178 |
| 6 | 0 | 1 | 400 | 85.25 | 203.2 | 54.25 | 31 | Y | 6 | 267.626 | 2830.02 | 17.047 | 0.07248 |
| 7 | 1 | 1 | 450 | 60.5 | 254 | 38.5 | 22 | Y | 5 | 230.765 | 2843.894 | 12.837 | 0.427028 |
| 8 | 0 | 1 | 400 | 85.25 | 203.2 | 54.25 | 31 | Y | 7 | 282.898 | 2834.179 | 13.868 | 0.248244 |
| 9 | 0 | 1 | 400 | 85.25 | 203.2 | 54.25 | 31 | Y | 7 | 278.075 | 2833.15 | 14.394 | 0.189505 |
| 10 | 1 | 1 | 350 | 60.5 | 152.4 | 38.5 | 22 | Y | 5 | 216.253 | 2826.062 | 15.089 | 0.285843 |
| 11 | 1 | 1 | 350 | 110 | 152.4 | 70 | 40 | N | 7 | 302.04 | 2828.571 | 14.976 | 0.032163 |

#### *4.1.1. Effects of Arc Current, Total Plasma Gas Flow, and Standoff Distance on Particle Temperature (Tp) and Velocity (Vp)*

Main effects plots, Figure 22, show the effects of arc current, total plasma gas flow, and standoff distance on Tp and Vp. Changes of < 20 degrees were seen in Tp. This small change in temperature is negligible. On the other hand, Vp was affected and significantly increased with increasing arc current, increasing total plasma gas flow, and decreasing standoff-distance. The DOE center points aligned nicely with the straight trend lines, suggesting that the relationship between these parameters and Vp are linear.

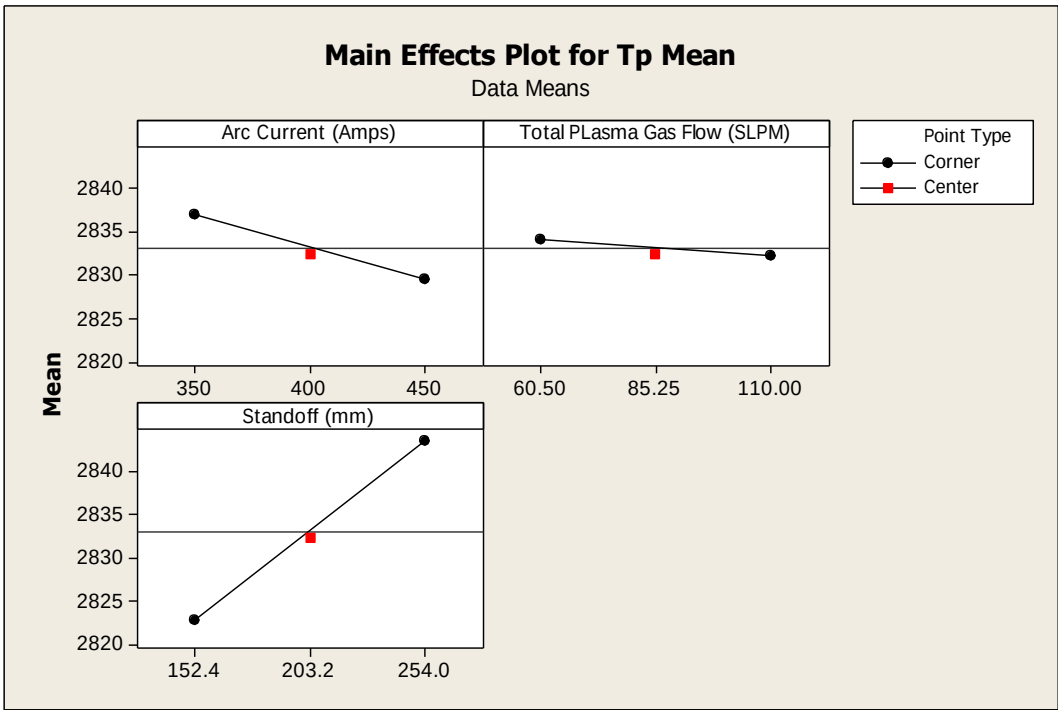


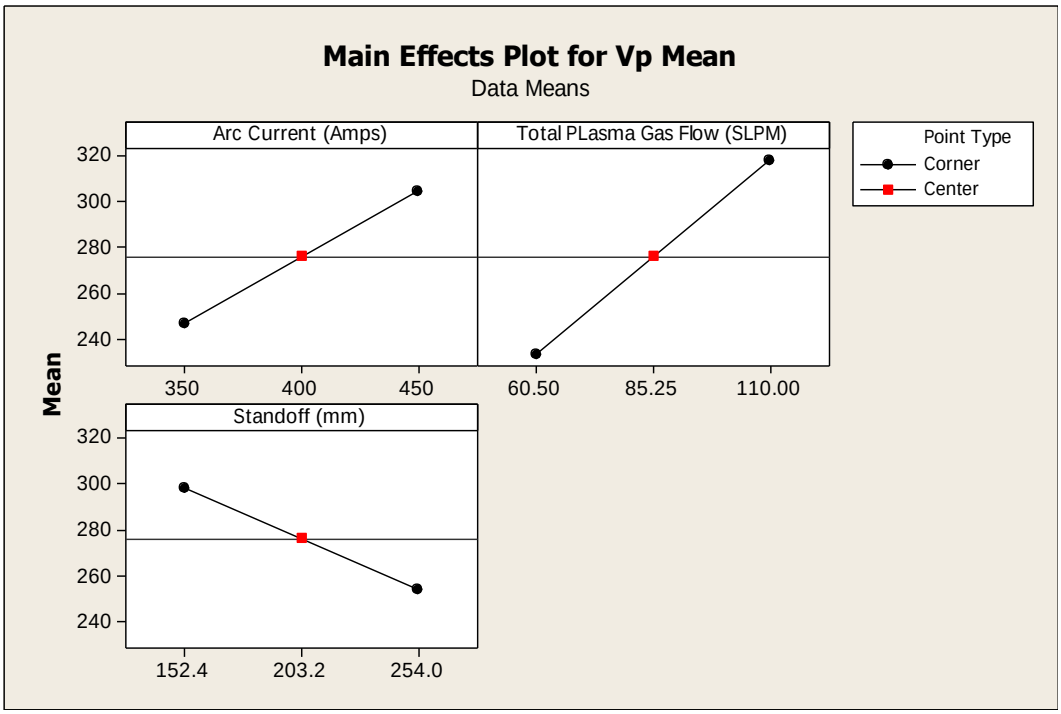


**Figure 22: Effects of arc current, total plasma gas flow, and standoff distance on particle temperature and velocity.**

### *4.1.2. Effects of Arc Current, Total Plasma Gas Flow, Standoff Distance on Sheet Resistance*

ANOVA analysis for sheet resistance as well as corresponding main effects and interaction plots are shown in Table 5 and Figure 23, respectively.

**Table 5: ANOVA analysis for sheet resistance**

| Estimated Effects and Coefficients for Sheet Resistance (ohms/square) | | | | | |
|---|---|---|---|---|---|
| **Term** | **Effect** | **Coefficient** | **SE Coefficient** | **T** | **P** |
| Constant | | 0.2986 | 0.03164 | 9.44 | 0.011 |
| Arc current (amps) | 0.4016 | 0.2008 | 0.03164 | 6.35 | 0.024 |
| Total plasma gas flow (SLPM) | 0.1704 | 0.0852 | 0.03164 | 2.69 | 0.115 |
| Standoff (mm) | -0.3110 | -0.1555 | 0.03164 | -4.92 | 0.039 |
| Arc current (Amps)* Total plasma gas flow (SLPM) | 0.2909 | 0.1455 | 0.03164 | 4.60 | 0.044 |
| Arc current (amps)*Standoff (mm) | -0.1886 | -0.0943 | 0.03164 | -2.98 | 0.096 |
| Total plasma gas flow (SLPM)*Standoff (mm) | -0.3415 | -0.1708 | 0.03164 | -5.40 | 0.033 |
| Arc current (amps)* Total plasma gas flow (SLPM)* Standoff (mm) | -0.4746 | -0.2373 | 0.03164 | -7.50 | 0.017 |
| Ct Pt | | -0.1285 | 0.06058 | -2.12 | 0.168 |

| | | |
|---|---|---|
| S = 0.0894782<br>R-Sq = 98.97% | R-Sq (adj) = 94.84%<br>R-Sq (pred) = *% | PRESS = * |

| Source | | F | P |
|---|---|---|---|
| Main effects | | 23.90 | 0.040 |
| | Arc current (amps) | 40.29 | 0.024 |
| | Total plasma gas flow (SLPM) | 7.25 | 0.115 |
| | Standoff (mm) | 24.16 | 0.039 |
| 2-Way interactions | | 19.72 | 0.049 |
| | Arc current (amps)* total plasma gas flow (SLPM) | 21.14 | 0.044 |
| | Arc current (amps)* standoff (mm) | 8.89 | 0.096 |
| | Total plasma gas flow (SLPM)* standoff (mm) | 29.14 | 0.033 |
| 3-way interactions | | 56.27 | 0.017 |
| | Arc current (Amps)* total plasma gas flow (SLPM)* standoff (mm) | 56.27 | 0.017 |
| | Curvature | 4.50 | 0.168 |

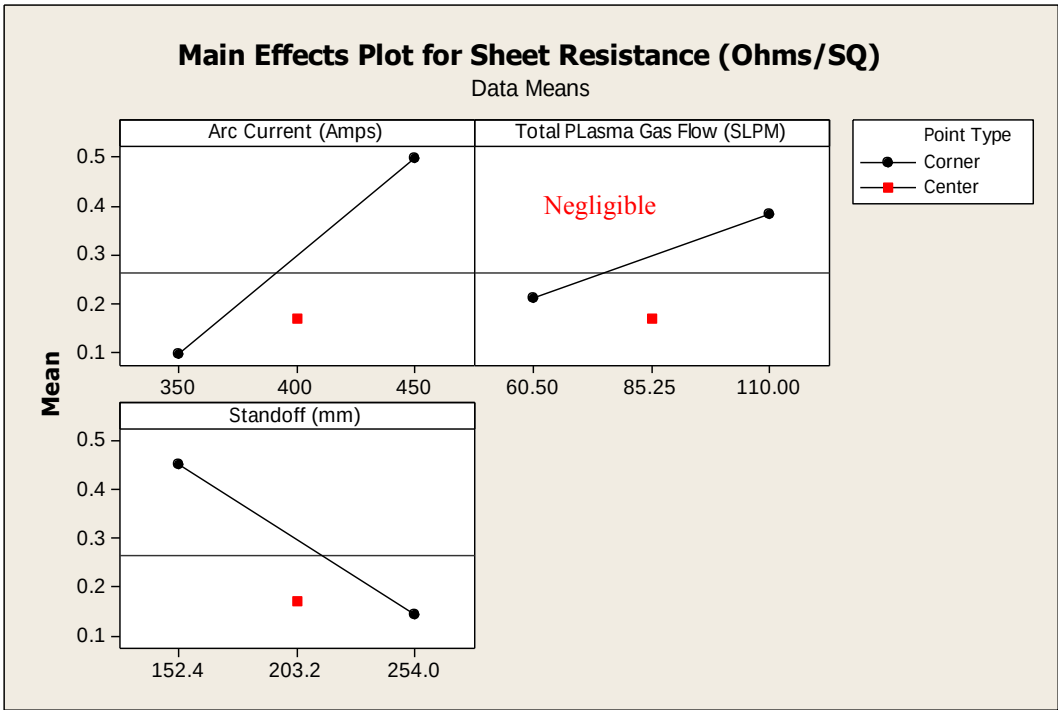


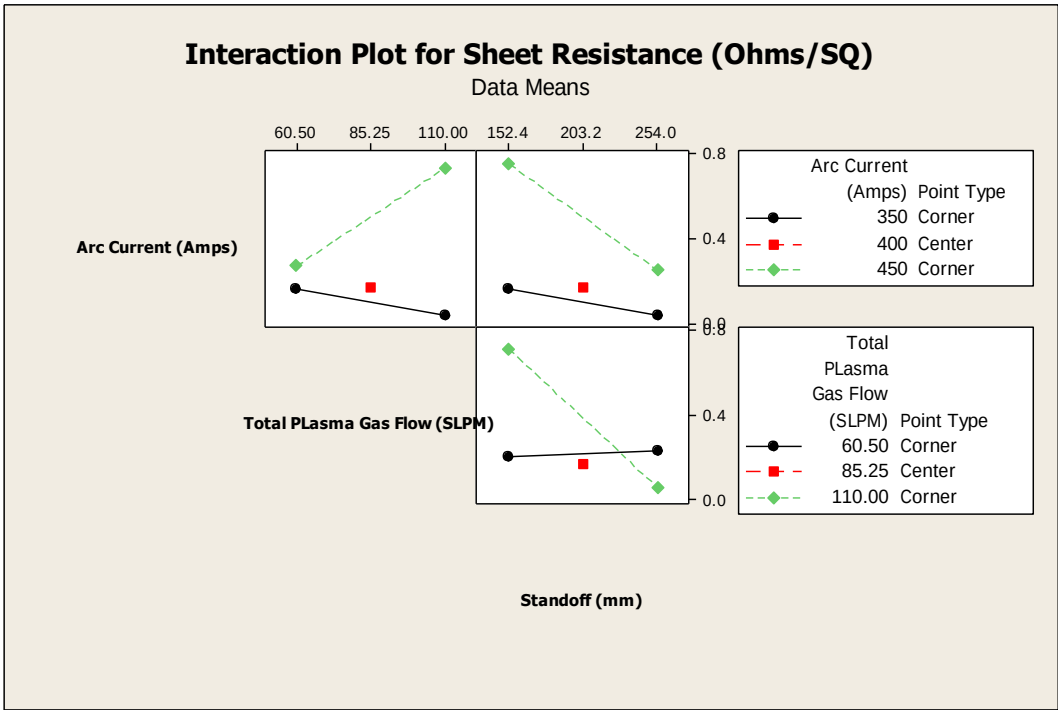


**Figure 23: Main effects of arc current, total plasma gas flow, and standoff distance as well as their interactions on sheet resistance, calculated using the data obtained from the DOE in MiniTab.**

From this analysis, we can say with 95% confidence ($P < 0.05$) that:

- The main effects for sheet resistance are arc current and standoff distance.
  - ↑arc current ↑sheet resistance
  - ↑standoff distance ↓sheet resistance
- Two interactions terms also affect sheet resistance: the interaction of arc current and total gas flow and the interaction of standoff distance and total gas flow.
  - (*high* arc current*↑total gas flow) ↑sheet resistance significant effect
    (*low* arc current*↑total gas flow) ↓sheet resistance little effect
  - (*high* total gas flow*↑standoff dis) ↓sheet resistance significant effect
    (*low* total gas flow*↑standoff dis) ↑sheet resistance negligible effect

The general trend is that the sheet resistance increases with increasing arc current and decreasing standoff distance. It is very probable that increasing arc current increases the in-flight particle oxidation and the inter-pass coating oxidation, and thus would increase the sheet resistance. Similarly, decreasing the standoff distance would also increase the inter-pass coating oxidation (because the hot plume would be closer to the coating and the substrate), and thus would increase the sheet resistance. Total gas flow alone does not have a significant effect on sheet resistance. However, the combination of total gas flow with high arc current or with long standoff distance does significantly affect sheet resistance.

In summary, the mean sheet resistance values as a function of arc current, total plasma gas flow, and standoff distance are shown in a cube plot in Figure 24. The lowest sheet resistance value was produced by conditions located at the edge of the DOE space, where the APS parameters are the least energetic (lowest arc current, lowest total plasma gas flow and longest standoff distance). Thus, we recommended that a second DOE be conducted to further optimize the APS process parameters by exploring lower energy process conditions.

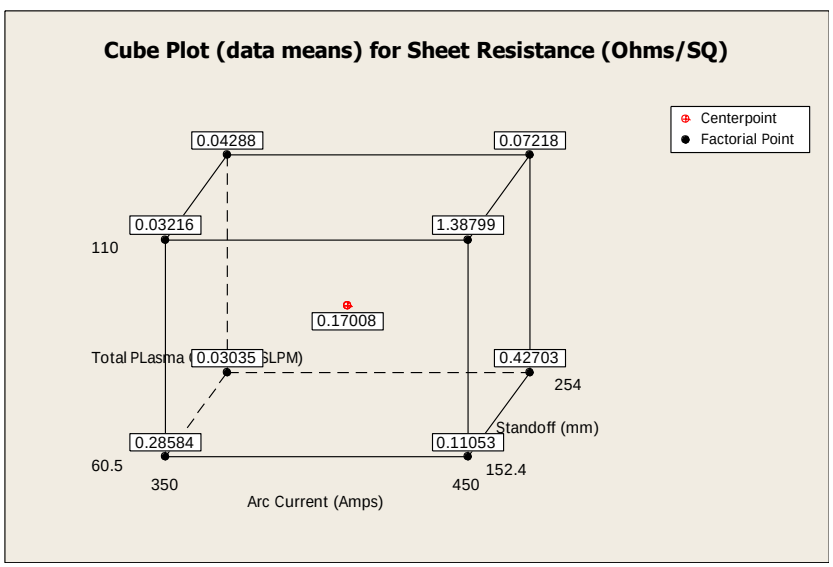


**Figure 24: Cube plot showing sheet resistance (ohms/square) as a function of arc current, total plasma gas flow, and standoff distance. The point with the lowest sheet resistance value is at the edge of the DOE space, where the APS conditions are the least energetic (lowest arc current, lowest total plasma gas flow and longest standoff distance). Additional exploration of lower energy process conditions is needed.**

The lowest two sheet resistances identified in the DOE above were associated with sample 1 and 3. In both cases, the film thickness (step height) was measured: 15.8±5μm for sample 1 and 25.9±5μm for sample 3. These data were used to convert the two sheet resistances to electrical resistivity values, 47.95μΩ cm for sample 1 and 111.07μΩ cm for sample 3. This still represents a high resistivity when compared to the reported bulk Mo resistivity value of 5.5 μΩ cm [7]. Thus, we speculated that a large amount of porosity and oxide may still exist in the thermal sprayed Mo coating. It should be noted that the electrical resistivity from the Phase II condition (47.95 μΩ cm) is a significant improvement from the Phase I condition (301.6 μΩ cm).

#### *4.1.3. Optimal APS coatings on N and P-type Bismuth Telluride*

Sample 1—sprayed with arc current of 350 Amps, total gas flow of 60.5 SLPM (38.5 SLPM Ar and 22 SLPM He), and stand-off distance of 10”—had the lowest electrical resistivity value. Thus, the spray condition used to prepare sample 1 was used to prepare Mo coatings on N- and P-type Bi-Te substrates, as shown in Figure 25. Both substrates were coated successfully.

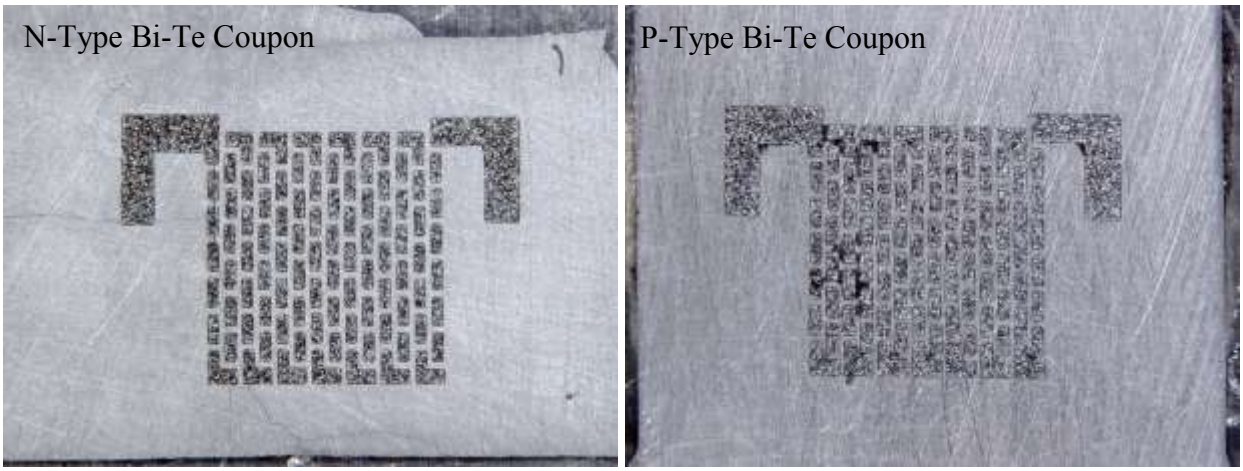


**Figure 25: Mo coatings (36μm powder size, 10 passes) produced using the optimized APS process parameters on the N-type (left) and P-type (right) Bi-Te coupons.**

FIB/EDS analysis was used to examine the solidification mode of Mo coating and the coating/substrate interface for both P-type and N-type Bi-Te substrates.

***Molybdenum Coatings on N-Type Bi-Te Substrates***

SEM images of the sprayed Mo coating (36μm powder size, 4 passes) on an N-type Bi-Te substrate (Figure 26) show that the substrate and the Mo coating are very rough and non-uniform.

FIB cross-section images are shown in Figure 27. The FIB cut intersected both the Mo splats and the substrate. A high magnification SEM image of the Mo splats shows dendritic solidification of the Mo, as seen in Figure 27. This coating exhibits less coating porosity and fewer voids at the coating/substrate interface when compared to the Phase I coating. Figure 28 shows EDS maps of the FIB cross-section. Distinct regions of Mo coating as well as Bi, Te, and Se containing

substrate can be seen. Thus, it was concluded that no significant chemical interaction occurred between the coating and the substrate.

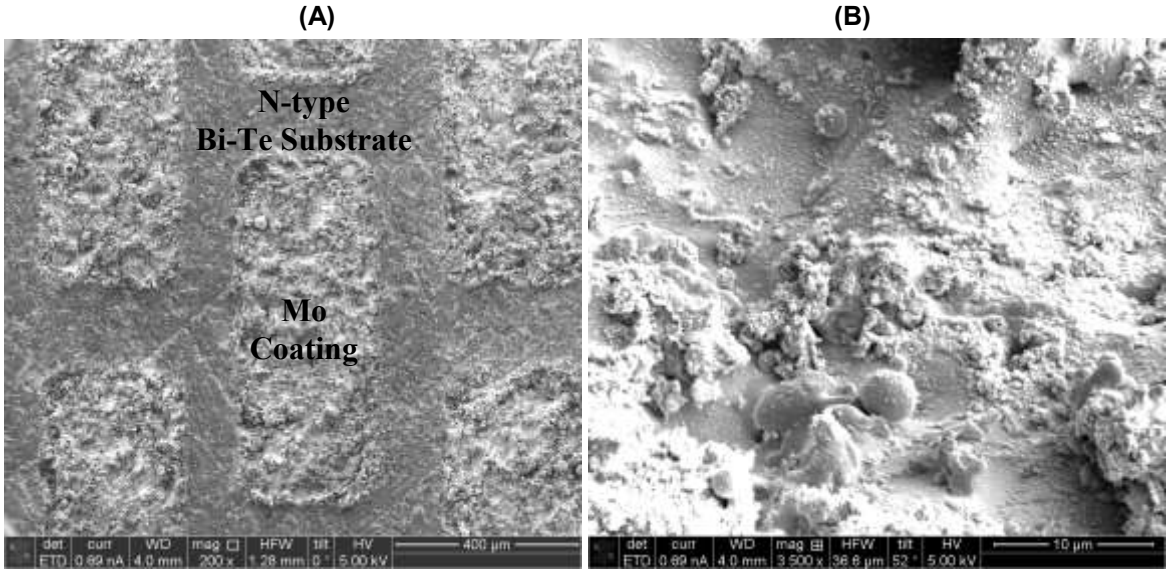


**Figure 26: SEM images of the Mo coating on an N-type Bi-Te substrate. The substrate and coating surface are rough. The coating surface is non-uniform. A) Image showing good feature and edge retentions of the coating. Some large Mo droplets can also be seen in the coating. B) High magnification SEM image showing splats and condensation at the coating surface.**

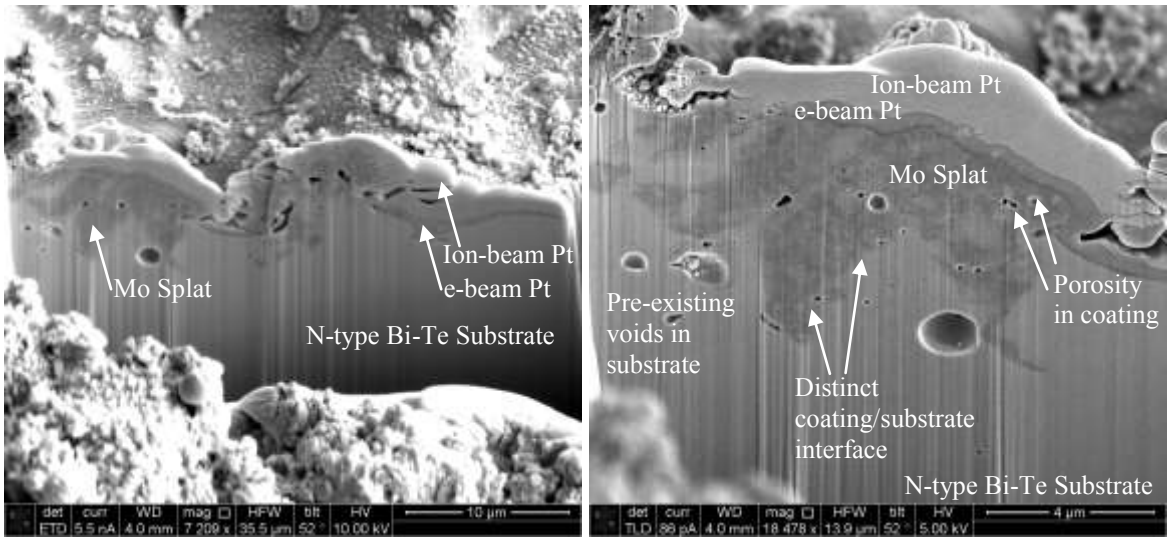


**Figure 27: A) SEM image of FIB cross-section of the Mo coating on an N-type Bi-Te substrate. B) High magnification SEM image of the far left corner of the cross-section. This Mo structure is likely from one or two splats. It penetrated deep into the substrates and exhibited dendritic solidification mode.**

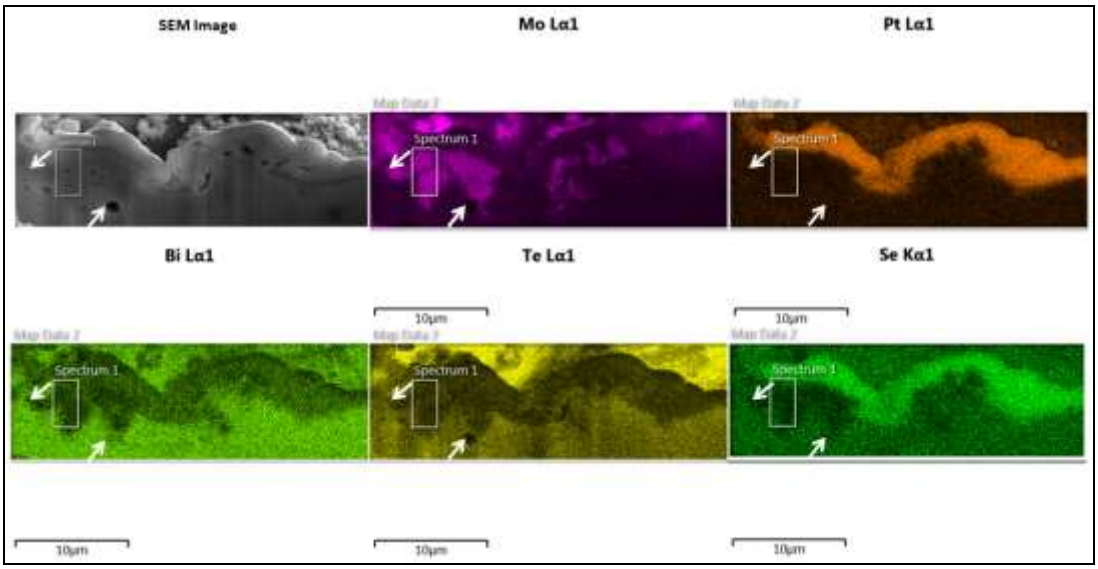


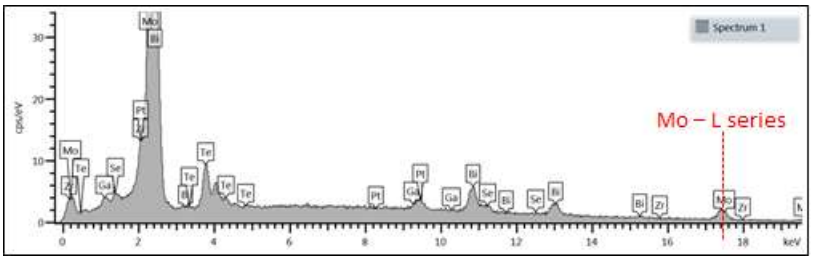


**Figure 28: EDS analysis of FIB cross section of Mo on N-type Bi-Te substrate, showing distinct regions including: Pt protective layer on the coating surface, Mo in the coating, and Bi, Te, and Se in the substrate. No significant mixing was observed at the coating/substrate interface.**

Metallographic cross-sections of the Mo on the N-type Bi-Te substrate were prepared. The cross section showed that the coating exhibited the expected lamellar microstructure. The particles were fully molten when they impacted the substrate and they deformed creating a lamellar structure of splats containing columnar grains, as shown in Figure 29. The Mo coating is approximately 10±5µm thick. The bare substrate contained sub-surface cracked and voids (bottom left image of Figure 29) prior to coating deposition. Micro-voids were found within the splats and at the splat boundaries. No dendrite structures (shown previously in Phase I) were observed within the splats. This suggested that the optimized spray condition from Phase II has decreased energy as compared to those from Phase I. This microstructure is more desirable.

It should be noted that significant amount of voids were observed immediately under the coating as shown by the top left and top right image in Figure 29. We expect that these voids were formed by gas bubbles arising from Te vaporization in the substrate. Tellurium has a low vapor pressure. It vaporizes at 250°C [9]. Thus, Te likely vaporized during the thermal spray coating process as the molten Mo particles impacted the Te containing substrate. Cracks were also found radiating from these voids. These voids and their associated cracks can significantly increase the coating electrical resistivity. Thus, it is recommended that aggressive substrate cooling, using liquid $CO_2$, be studied in the future. Such aggressive substrate cooling is likely to minimize Te vaporization and should create a Mo coating with a more intact coating substrate interface.

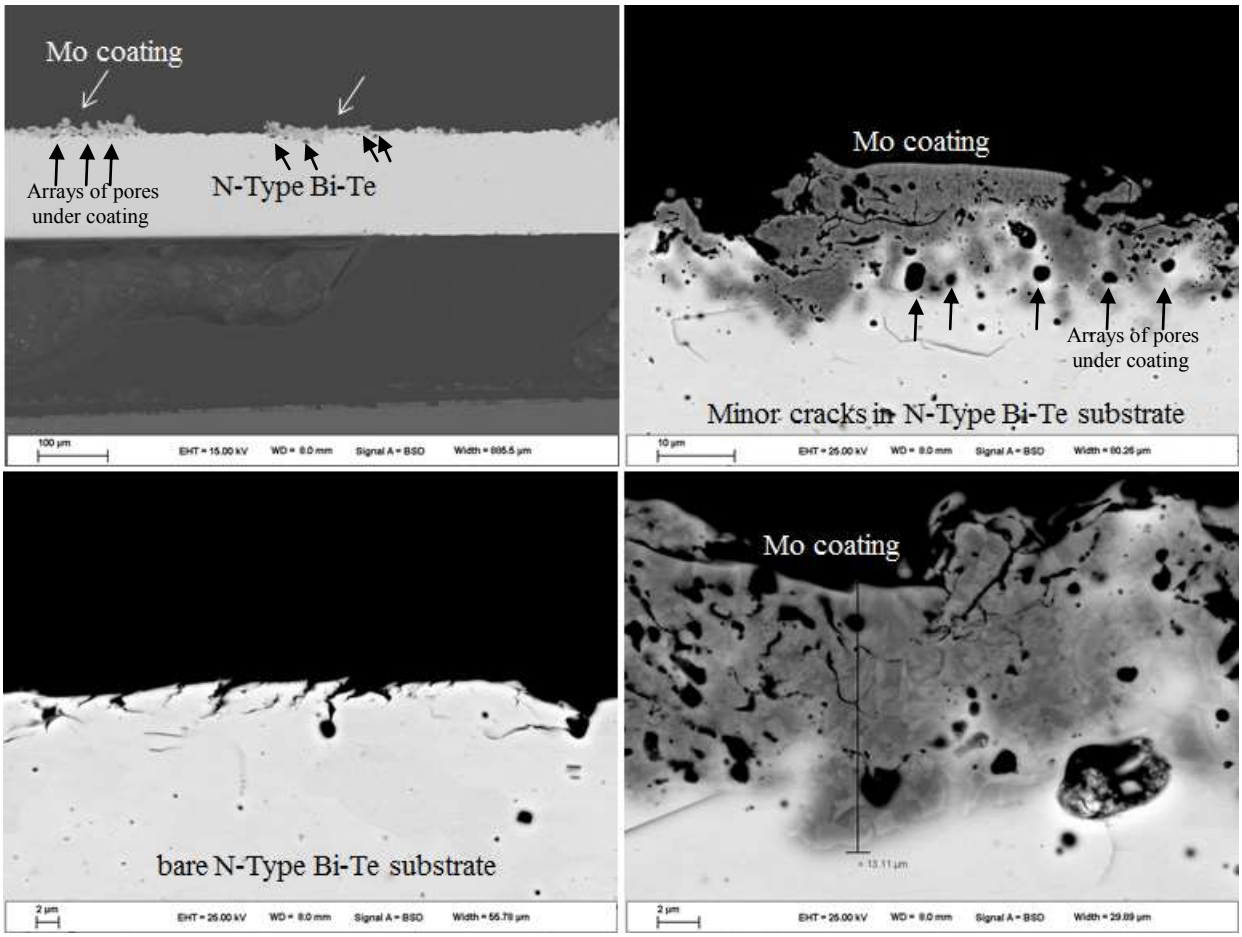


**Figure 29: Back-scattered electron images of polished coating cross-sections showing Mo on an N-Type Bi-Te substrate. The coating is approximately 10±5μm thick. The bare substrate had sub-surface cracks and voids (bottom left picture) prior to Mo deposition. The coating (top and bottom right images) exhibits characteristic lamellar structure with columnar grains inside the Mo layers. This is typical of coatings produced by thermal spray process. As before, voids were found immediately beneath the coating. These are believed to arise from gas bubbles produced by Te vaporization during the Mo deposition process.**

*Molybdenum Coatings on P-Type Bi-Te Substrates*

An SEM image showing the sprayed Mo coating (36µm powder size, 4 passes) on a P-type Bi-Te substrate (Figure 30) reveals that substrate and Mo coating are very rough and non-uniform. Unlike the N-type Bi-Te, the P-type Bi-Te coupons were significantly more brittle and contained extensive porosity and pre-existing cracks.

A FIB cross-section image is also shown in Figure 30. This image of the Mo splats shows dendritic solidification in the Mo. It also shows voids within the Mo splats, at the splat boundaries, and at the coating/substrate interface. Voids and grain boundary cracking within the P-type Bi-Te substrates were also seen. Figure 31 showed EDS analysis of the FIB cross-section. Distinct regions of Mo coating as well as Bi, Te, and Sb containing substrate can be seen. It should be noted that the Te and Sb peaks nearly overlapped each other, thus the elemental mapping of the Te and Sb had similar appearance. These data showed that no significant coating/substrate chemical interaction occurred.

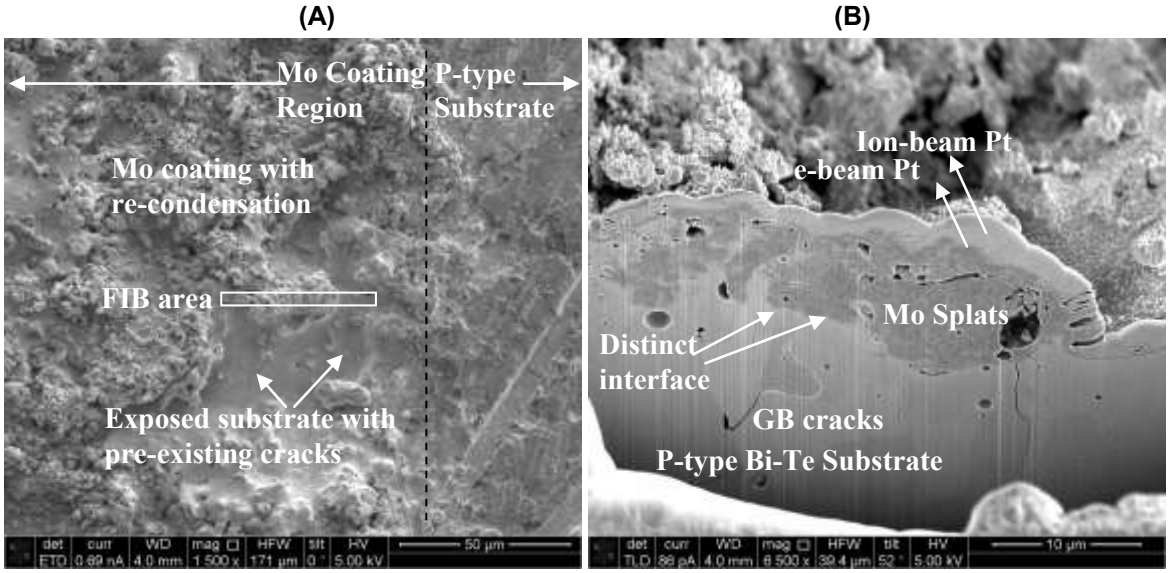


**Figure 30: SEM images showing the Mo coating on a P-type Bi-Te substrate. A) SEM image showing a top view of the coating. Exposed substrate areas with pre-existing cracks can be seen. The cross-section was performed in the area indicated by the box in the left image. B) The cross-section showing Mo splats penetration, deep into the substrate. Mo exhibited dendritic solidification. Voids are observed in the Mo coating as well as at the splat boundaries, the coating/substrate interface, and in the substrate.**

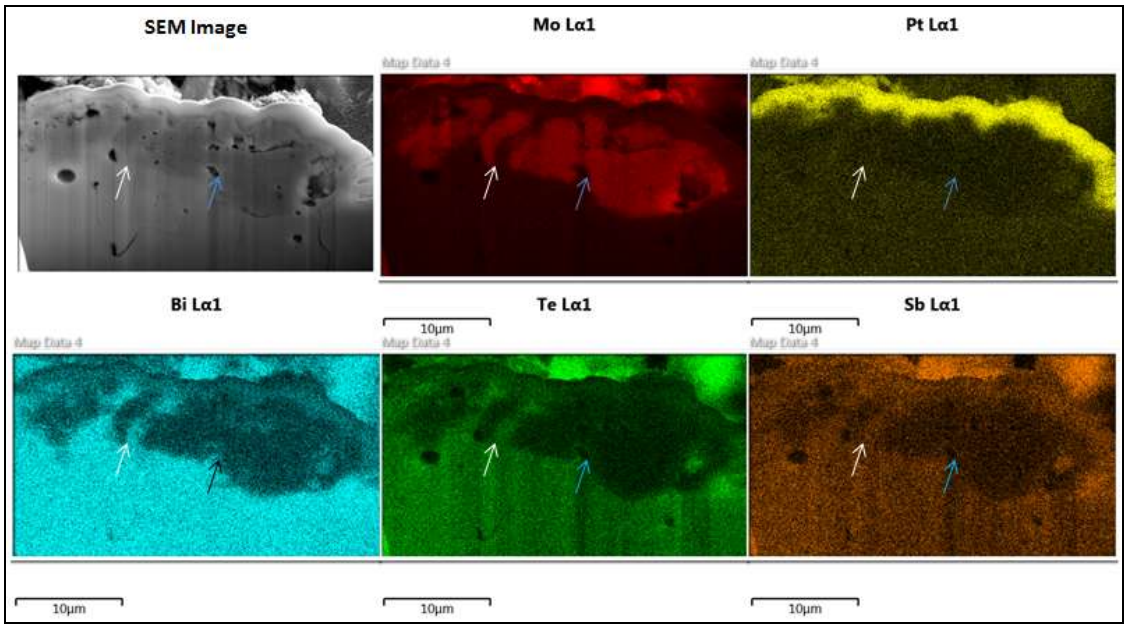


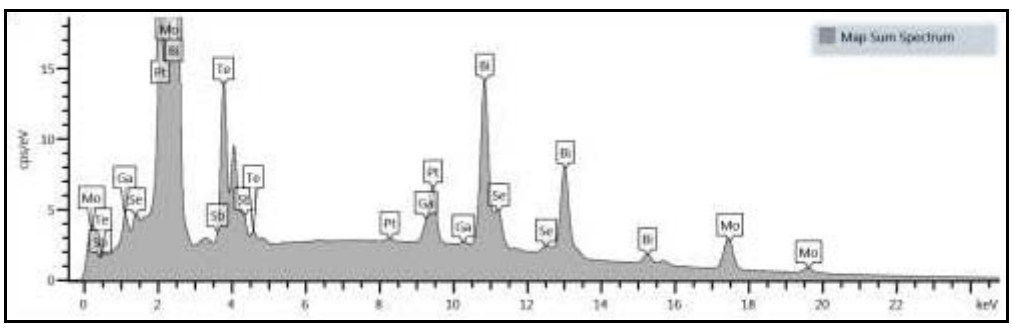


**Figure 31: EDS maps taken from the FIB cross section of the Mo coating on the P-type Bi-Te substrate, showing distinct regions, including the Pt protective layer on the coating surface, Mo in the coating, and Bi, Te, and Sb in the substrate. No significant mixing was observed at the coating substrate interface.**

Metallographic cross-sections of the Mo coating on the P-type Bi-Te substrate were prepared. The cross sections showed that Mo particles were fully molten when they impacted the substrate, leading to the expected lamellar structure formed of Mo splats columnar grains, as seen in Figure 32. The bare substrate exhibited sub-surface cracking and contained numerous micro-voids (bottom left image of Figure 32) prior to coating deposition. Micro-voids were found within the splats and at the splat boundaries. No dendrite structures, as observed previously in the Phase I coatings, were found within the Mo splats with the exception of Mo particles which solidified prior to reaching the substrate and landed on top of the coating (top right picture of Figure 32).

Similar to the Mo coating on N-type Bi-Te, a significant number of voids were observed immediately under the coating on the P-type Bi-Te, as seen in Figure 32 top left and right images. These voids are believed to be gas bubbles formed by Te vaporization during deposition. As before, cracks were observed radiating from these voids. Because the P-type substrate is much more brittle than the N-type substrate, cracking underneath the coating was more extensive.

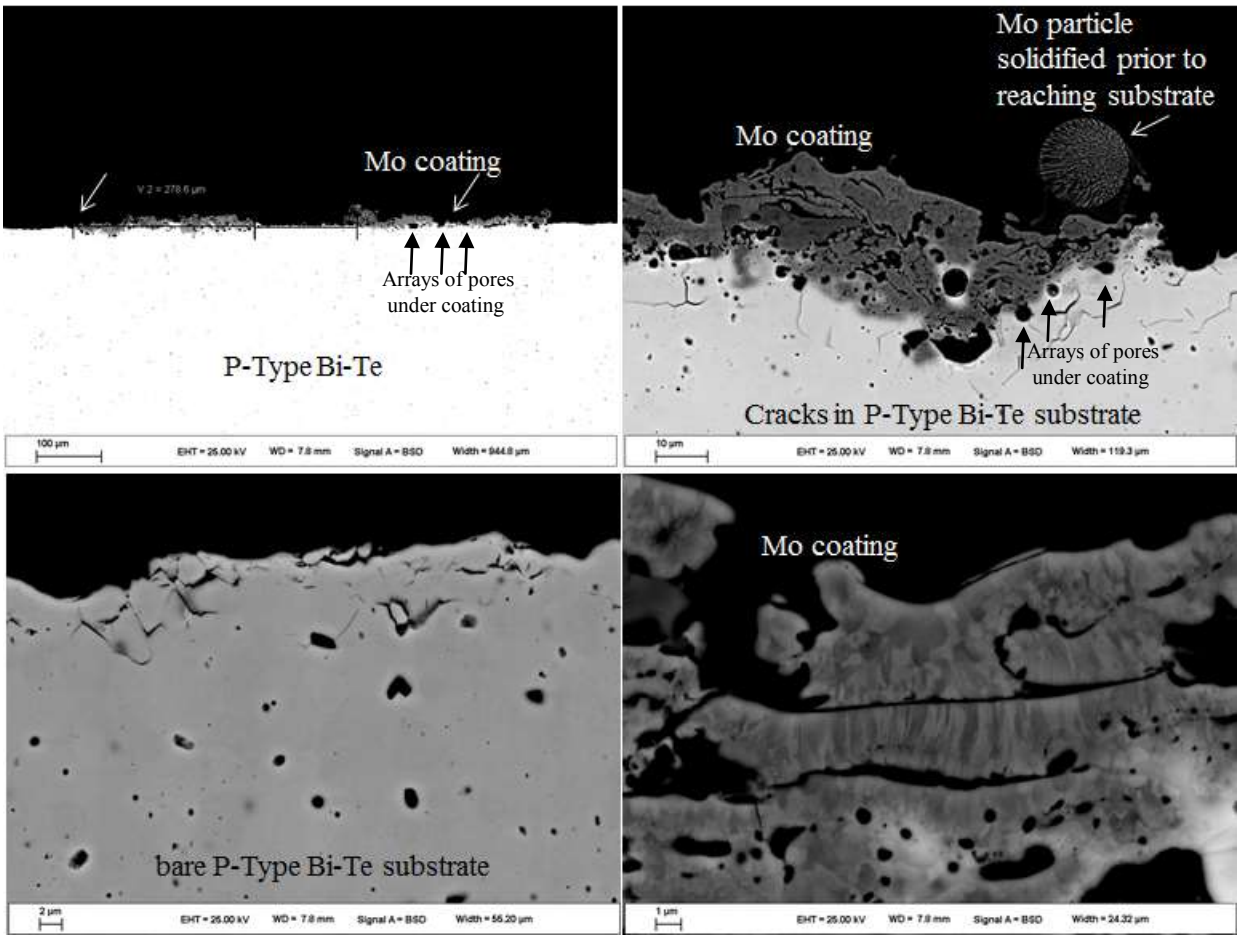


**Figure 32: Back-scattered electron images of polished metallographic cross-sections showing the Mo coating on a P-Type Bi-Te substrate. The bare substrate had sub-surface cracks and numerous voids (bottom left picture) prior to coating deposition. The coating (top and bottom right images) exhibits a lamellar microstructure characteristic of sprayed coatings. Voids were found within the splats and at the splat boundaries. The top right picture also shows a particle that solidified dendritically prior to reaching the substrate. Voids were found immediately under the coating. These are believed to be gas bubbles formed by Te vaporization during the spray process.**

## 4.2. Phase II Coating Process Optimization Summary

Coating process optimization was conducted using a Design of Experiment (DOE) to identify process conditions that produced a Mo coating with the lowest electrical resistivity. The best spray conditions identified were arc current of 350 Amps, total plasma gas flow of 60.5 SLPM (38.5 SLPM Ar and 22 SLPM He), and a stand-off distance of 10" or 254mm. The electrical resistivity of the coating produced was determined to be 47.95 μΩ cm, which was a significant improvement from the Phase I coating of 301.6 μΩ cm. The lowest sheet resistance value was produced by conditions located at the edge of the DOE space, where the APS parameters were the least energetic (lowest arc current, lowest total plasma gas flow and longest standoff distance). This suggested that further reducing the spray plume energy could further improve the coating. Thus, another DOE was conducted in Phase III to explore less energetic APS process parameters.

The optimized spray condition from Phase II was used to prepare Mo coatings on N- and P-type Bi-Te substrates. Using FIB/EDS analysis, it was determined that there was no coating/substrate interaction with either the N- or P-type Bi-Te substrates. The microstructure of the coatings still exhibits some pores within the splats, at the splat boundaries, and at the coating/substrate interface. Back-scattered electron images of coating cross-sections revealed the expected coating microstructure of lamellar splats containing columnar grains. Round pores and cracks radiating from the pores were found immediately under the Mo coating and were associated with Te vaporization during the spray process. Vaporization is thought to occur when the molten Mo droplets (2623°C) transferred their heat of solidification to the substrate at the moment of impact. We expect that tellurium vaporization can be mitigated by aggressively cooling the substrate during the deposition process. Thus, it was recommended that substrate cooling using liquid $CO_2$ be explored. Liquid $CO_2$ cooling is a well-known technique for cooling substrates in the thermal spray community and this capability exists at Sandia's Thermal Spray Research Laboratory.

# 5. PHASE III – DEMONSTRATION OF AN APS MO INTERCONNECT ON THERMOELECTRIC MODULES

The final phase of the project involved a second DOE to further optimize the APS process condition. This refined process condition was used to prepare Mo interconnects on actual thermoelectric modules. The goals of this phase were to pass a circuit test and produce parts with an electrical resistance approaching the theoretical electrical resistance values.

The thermoelectric stack is composed of N-type and P-type Bi-Te pillars in an insulating cement matrix. Both the P- and N-type Bi-Te were made using a powder metallurgy process and then cut into pillars. The P-type Bi-Te is significantly more brittle than the N-type. Voids and cracks are expected in these pillars because the powder metallurgy process does not produce fully dense materials. Voids are also present in the cement filling that holds the thermoelectric stack together. Once the Mo coating was deposited on both ends of the thermoelectric stack, circuit testing was performed. All thermoelectric module fabrication, mask alignment on the modules, Ti/Au deposition, circuit testing, and circuit repair were performed by Catherine Sobczak (01832).

## 5.1. Second DOE for APS Process Optimization

As discussed in Phase II, the optimal APS process condition identified in the first DOE was produced by the least energetic spray condition investigated. Thus, a second DOE was conducted to explore even lower energy spray conditions. In the first DOE, the standoff distance, arc current, and total gas flow were varied. The He/Ar in the plasma forming gas was held constant. The second DOE varied arc current, Ar/He ratio in the plasma gas, and total plasma gas flow. Standoff distance was held constant at 254mm. Particle temperature, particle velocity, particle diameter, and sheet resistance were measured at each coating condition as shown in Table 6.

**Table 6: Results on Vp, Tp, Dp and Electrical Resistivity from refined DOE in Phase III**

| Run Order | Center Pt | Arc Current (I) | Ar/He Ratio | Total Flow (SLPM) | Ar Flow (SLPM) | He Flow (SLPM) | Vp Mean (m/s) | Tp Mean (m/s) | Dp Mean (µm) | Sheet Resistance (Ω/sqr) |
|---|---|---|---|---|---|---|---|---|---|---|
| 1 | 1 | 150 | 1.5 | 60.5 | 38 | 25 | 200 | 2851 | 16 | 0.0003 |
| 2 | 1 | 150 | 1.75 | 50 | 30 | 17 | 152 | 2860 | 14 | 0.00035 |
| 3 | 1 | 350 | 1.5 | 50 | 30 | 20 | 116 | 2870 | 12 | 0.0004 |
| 4 | 0 | 250 | 1.625 | 55.25 | 34 | 21 | 158 | 2854 | 14 | 0.0002 |
| 5 | 0 | 250 | 1.625 | 55.25 | 34 | 21 | 167 | 2851 | 15 | 0.0002 |
| 6 | 0 | 250 | 1.625 | 55.25 | 34 | 21 | 145 | 2861 | 13 | 0.0003 |
| 7 | 1 | 350 | 1.75 | 60.5 | 38 | 22 | 155 | 2851 | 14 | 0.00025 |

ANOVA analysis of this DOE did not identify any process factors that significantly affected sheet resistance. This may result from the extremely low measured values of sheet resistance. The sheet resistances reported above were near the measurement limit of the instrument. Nevertheless, an optimal condition identified by the DOE above is the center point condition because it exhibits the lowest sheet resistance and is reproducible. This condition is 10 passes of 36µm-sized Mo powders sprayed using an arc current of 250 Amps, 34 SLPM Ar and 21 SLPM

He gas flows, and standoff distance of 10” or 254mm. This condition was identified after the thermoelectric modules were sprayed and it was not used to prepare the modules described in Phase III. Instead the optimal condition from the Phase II DOE was used.

## 5.2. Preparation of Mo Coatings on Thermoelectric Modules

A functioning thermoelectric stack must have interconnects on both ends. Molybdenum coatings were prepared on each end of an assembled thermoelectric module, using the optimized APS process condition from Phase II.

### *5.2.1. Stack Fixture Design for APS Coating*

A fixture was needed to hold the thermoelectric modules and mask during the coating process. The fixture consisted of an Al back plate, a stack of thin $Al_2O_3$ plates, and an $Al_2O_3$ cover plate that compressed the entire assembly as shown in Figure 33 and Figure 34. The thin $Al_2O_3$ plates were used to accommodate variation in the thermoelectric stacks height.

Masks made from carbon-filled Kapton tape were manually aligned and applied to the thermoelectric modules. Double sided tape was used to secure the modules to the Al back plate of the fixture. The thin $Al_2O_3$ plates were then stacked around the modules. Kapton tape without adhesive was placed around the stacks and the cover plates were placed on top of the assembly. The final assembly of the modules, masks, and fixture is shown in Figure 35. Fixture design and mask alignment process were performed by Adrian Wagner (01833) and Catherine Sobczak (01832), respectively.

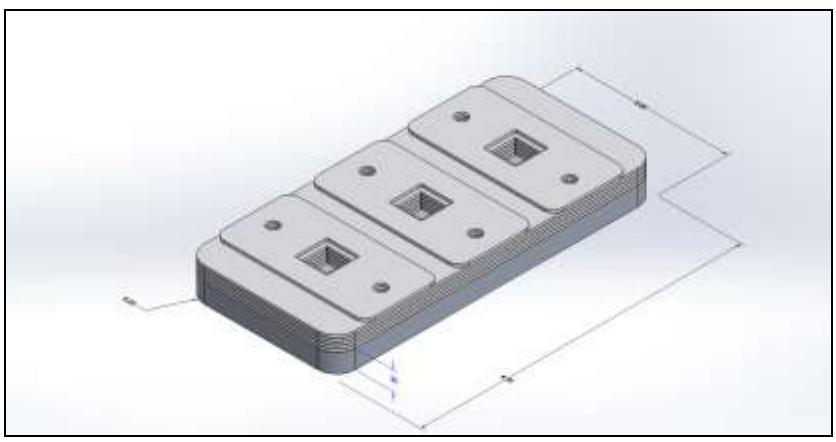

**Figure 33: 3D Solid Works drawing of the fixture designed to hold three thermoelectric stacks, shaped to fit into TSRL’s APS substrate holder.**

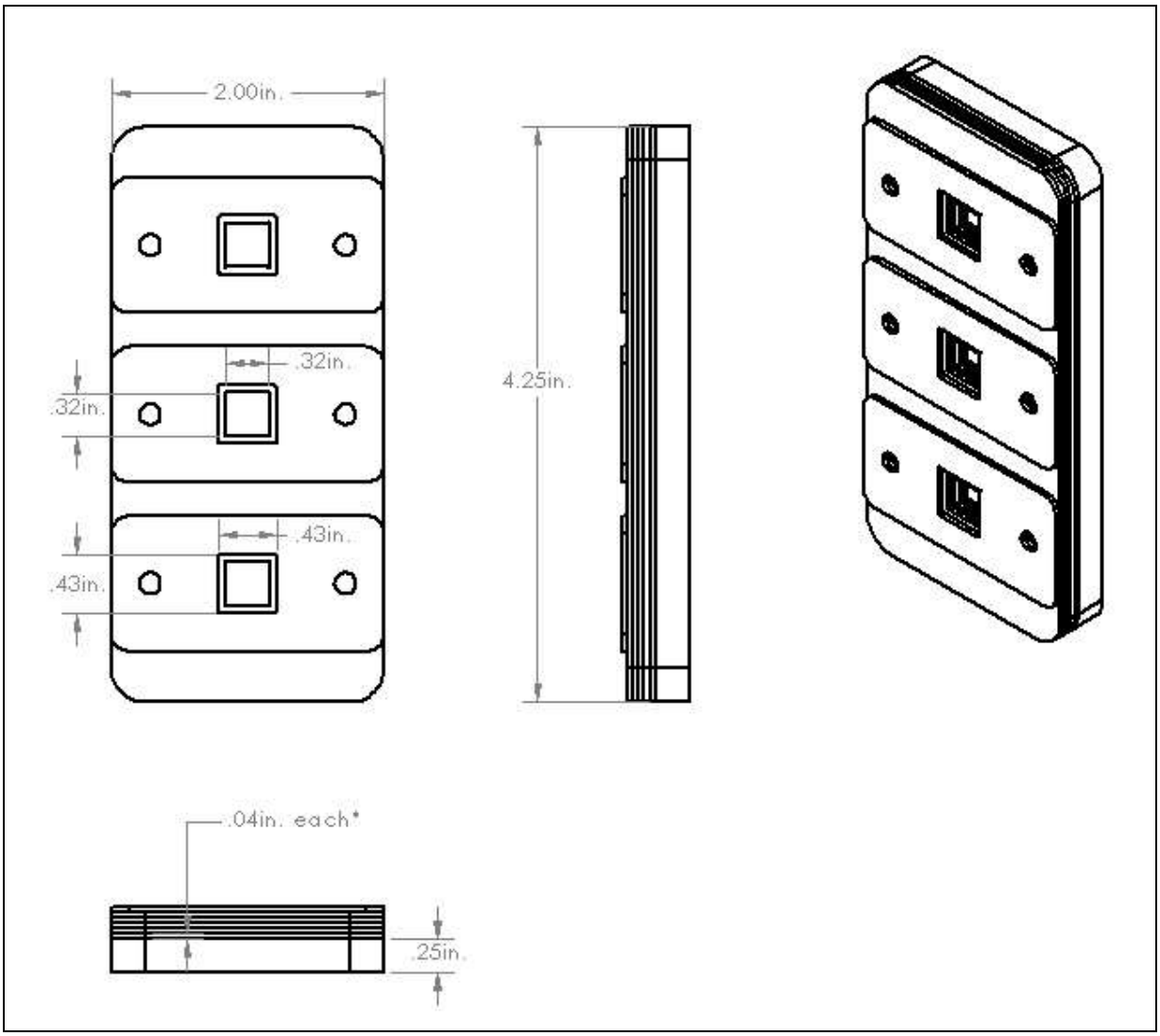


**Figure 34: Multiple views of the fixture designed to hold three thermoelectric stacks, shaped to fit into TSRL's APS substrate holder.**

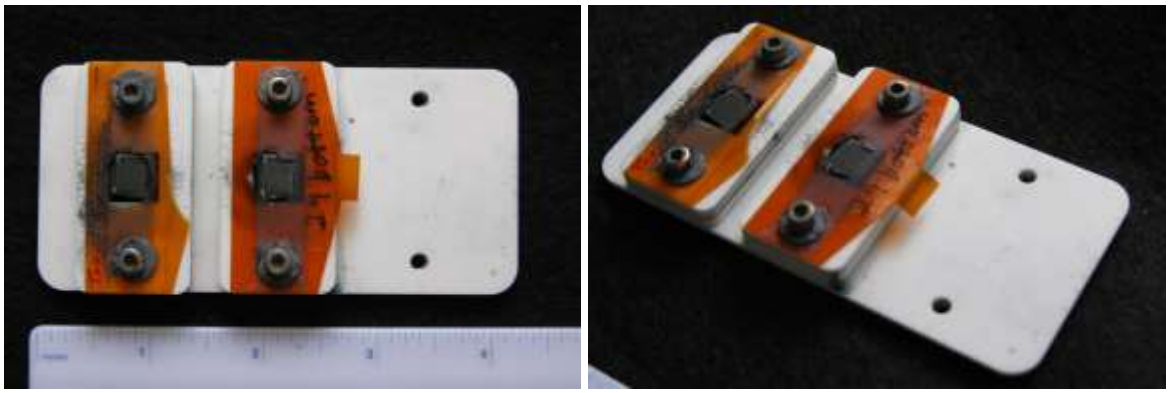

**Figure 35: Final assembly of the fixture. These two images were taken after spraying.**

### 5.2.2. Preparing an APS Mo Coating on Thermoelectric Modules

The thermoelectric modules (module #20 and #22), were sprayed using conditions from the Phase II DOE because the Phase III DOE had not yet been conducted. Specifically, Mo was sprayed using an arc current of 350 Amps, total plasma gas flow of 60.5 SLPM (38.5 SLPM Ar and 22 SLPM He), and standoff distance of 10" (254mm). The 36µm Mo powder identified in Table 3 was used for coating all thermoelectric modules. Each end of the thermoelectric module was masked and coated individually. The coating was applied with 10 passes. After the first end was coated, the modules were flipped, the uncoated side was masked, re-fixtured, and then sprayed with 10 passes.

During this process it was discovered that 20 spray passes created Mo coatings that were too thick and bridging on the mask was an issue. As the masks were removed, several interconnect pads detached from the modules and came off with the masks. These modules were polished to remove the defective Mo coating and will be recoated with only 10 passes of air plasma sprayed Mo at the beginning of FY14.

### 5.2.3. Thermoelectric Module Circuit Testing

After both ends of the thermoelectric modules were coated with Mo, the modules were electrically tested. An AC signal was applied to the stack using an LCR meter and total circuit resistance was measured. Failure to completely fill the interconnect features defined by mask with Mo coating will result in a failure during circuit testing. Bridging between interconnect features will result in circuit resistance much lower than theoretical value. The goal is to make a circuit with resistance approaching the theoretical resistance of 112Ω over the 6 mm long module assemblies and 150Ω over the 8 mm long module assemblies.

### 5.2.4. Circuit Repair

It was believed that the APS Mo coating was not completely continuous. Circuit repair done by depositing a thin Ti-Au layer on top of the APS Mo coating could greatly improve the conductivity by joining islands of Mo. Once it was determined that a complete circuit was made, Catherine Sobczak (01832) masked the Mo coated thermoelectric modules and plasma-sputtered a thin layer of Ti-Au on top of the Mo coatings on both ends of the modules. Subsequently, post-repair circuit testing was performed.

## 5.3. Circuit Testing Results

Images of the as-sprayed thermoelectric modules #22 and #20 are shown in Figure 36 and Figure 37. Stack #22 has well defined Mo features while #20 has some overlapping features. As shown in Table 7, the total circuit resistance across columns in the as-sprayed Mo coated modules #22 and #20 vary greatly between 20Ω and 4.3MΩ. Table 7 shows data for each of the 14 columns, numbered sequentially from left to right as shown in Figure 36 and Figure 37.

**Table 7: Column-by-column electrical resistance of as-sprayed Mo coatings from the first set of the thermoelectric module #22 and #20. The ideal resistance value across a column is ~20Ω.**

| Resistance across column | 1 | 2 | 3 | 4 | 5 | 6 | 7 | 8 | 9 | 10 | 11 | 12 | 13 | 14 |
|---|---|---|---|---|---|---|---|---|---|---|---|---|---|---|
| #22 | 91.24Ω | 3.65MΩ | 4.3MΩ | 26.7Ω | 22.8Ω | 1.25MΩ | 576Ω | 3.49MΩ | 3.5MΩ | 3.6MΩ | 2.5MΩ | 128.9Ω | OPEN | 2.0MΩ |
| #20 | 95.5Ω | 14Ω | 16.5Ω | 19.8Ω | 91.9Ω | 22.9Ω | 21.9Ω | 23.3Ω | OPEN | 24.2Ω | 36.6Ω | OPEN | 28.7Ω | 20.4Ω |

The resistance measured across the module after Ti-Au deposition circuit repair was 127.8Ω for module #22 and 47.5Ω for module #20 (low resistance due to bridging). Module #22 has shorter legs so its resistance of 127.8Ω is approaching theoretical value. This demonstrated success of air plasma sprayed Mo coating process for preparing thermoelectric module interconnects.

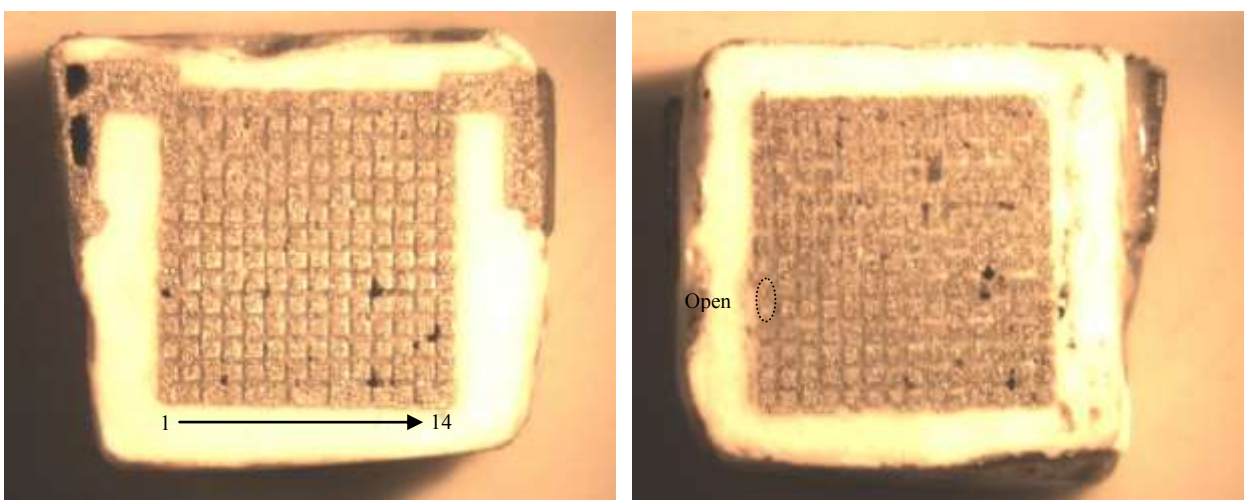


**Figure 36: Thermoelectric module #22 coated with Mo. The left image is the front side and the right image is the back side of the module. Macro-voids (dark spots) in the cement matrix can be seen. The Mo features were well defined and distinct. The resistance after Ti-Au deposition circuit repair was measured to be 127.8Ω, approaching the theoretical resistance of 112Ω for a module with 6 mm long legs.**

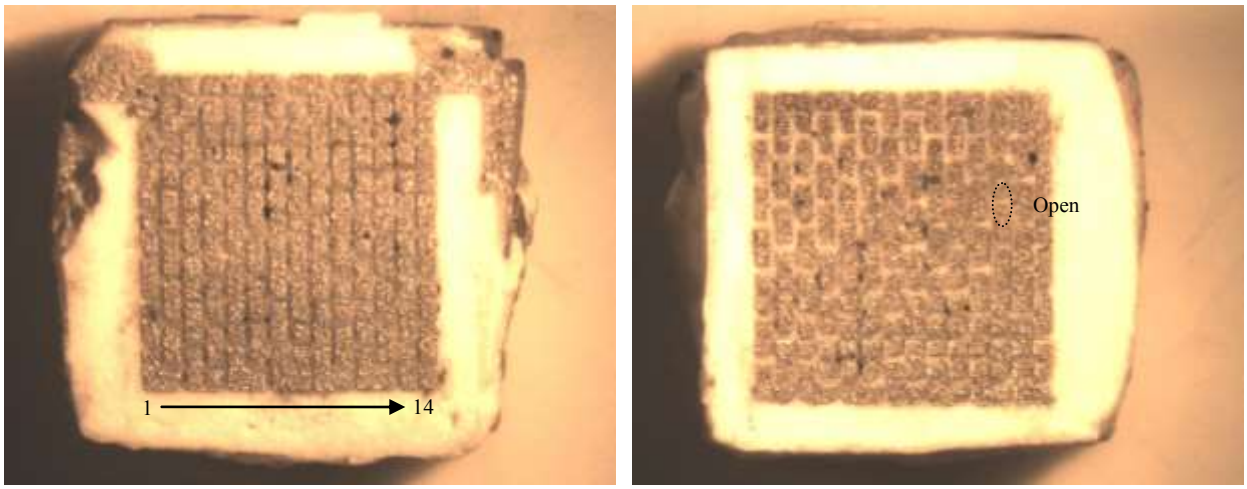


**Figure 37: Thermoelectric module #20 coated with Mo. The left image is the front side and the right image is the back side of the module. Macro-voids (dark spots) in the cement matrix can be seen. There were overlapping features in the Mo coating. The resistance after Ti-Au deposition circuit repair was measured to be 47.5Ω due to overlapping features.**

## 5.4. Microstructure of Air Plasma Spray Coating on Ti/Au Layer

A brief experiment to explore applying the Mo coating on top of a sputtered Ti/Au layer was conducted. It was postulated that air plasma spray process would force the existing Ti/Au layer into the Bi-Te substrate, creating better mechanical adhesion of the Ti/Au layer to the Bi-Te substrate. To test this hypothesis, a Ti/Au layer was sputtered through a Kapton tape mask onto the Bi-Te flats and a CoNiCrAlY coating was mistakenly, subsequently air plasma-sprayed on top of the Ti/Au layer. Although the CoNiCrAlY coating was mistakenly sprayed (instead of the Mo), it proved that an air plasma sprayed coating would not mechanically force the Ti/Au layer into the Bi-Te substrate.

Figure 38 shows SEM images of the CoNiCrAlY coating. The cross-section image shows that the Ti/Au layer conformed to the Bi-Te substrate and that the sprayed coating did not drive the Ti/Au layer into the substrate as intended. Compared to the cross-section images showing the interface where the air plasma sprayed Mo coating is embedded in the Bi-Te substrate (Figure 27 and Figure 29), the Ti/Au layer was not embedded in the Bi-Te substrate. This can also be seen clearly in the FIB/EDS maps (Figure 39), showing distinct regions of Au, CoNiCrAlY coating, and Bi-Te substrate.

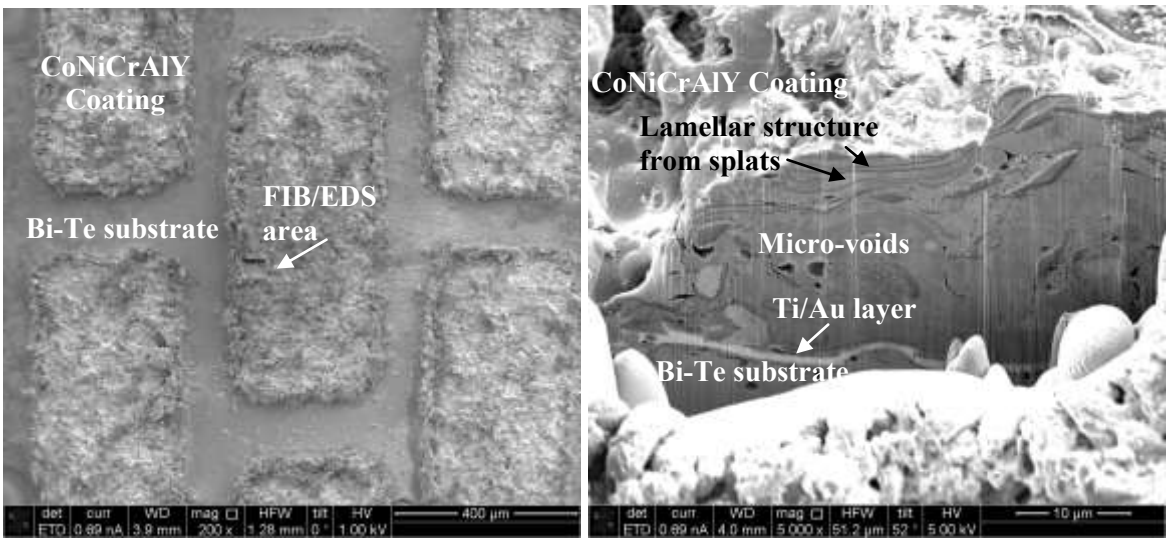


**Figure 38: SEM images of CoNiCrAlY coating and FIB cross-section of the CoNiCrAlY coating (22µm powder size, 13 passes) on sputtered Ti/Au (light-colored layer) on Bi-Te substrate.**

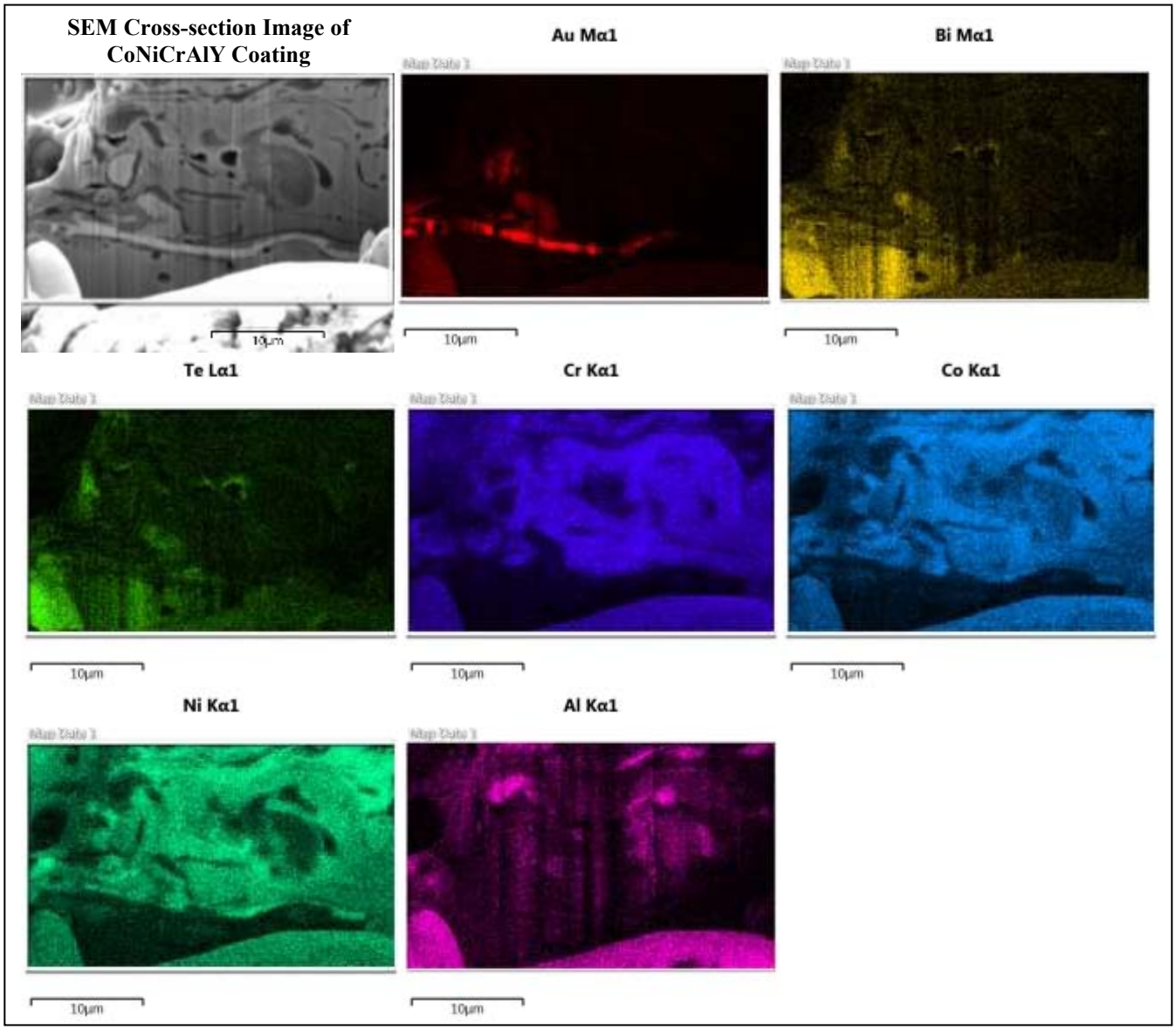


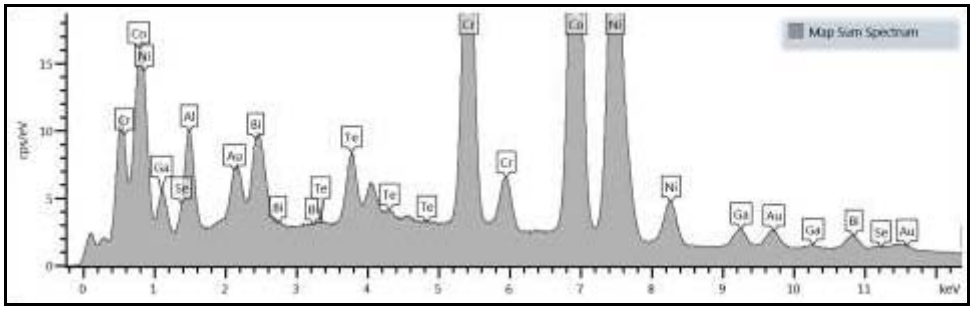


**Figure 39: EDS analysis of a CoNiCrAlY cross section (22.027µm powder size, 13 passes) on sputtered Ti/Au over a Bi-Te substrate, showing distinct regions of sputtered Au layer, CoNiCrAlY coating, as well as Bi and Te in the substrate. No embedding or significant mixing between the Au and the Bi-Te were observed at the interface.**

## 5.5. Phase III Thermoelectric Module Coating Summary

Molybdenum electrical interconnects were prepared on thermoelectric modules by air plasma spraying a 36µm sized Mo powder through a laser-cut mask made from carbon-filled Kapton tape. The Mo coating exhibited excellent feature and spacing retention (~170µm size) was adherent and produced electrical conductivity appropriate for the thermoelectric module application. Molybdenum interconnects were successfully prepared on thermoelectric modules using spray conditions determined previously from Phase II—arc current of 350 Amps, total plasma gas flow of 60.5 SLPM (38.5 SLPM Ar and 22 SLPM He), and a stand-off distance of 10" or 254mm. The addition of a Ti/Au layer on top of the Mo coating resulted in a module with an electrical resistivity of 128Ω, approaching a theoretical resistivity value of the 6mm leg module of 112Ω. The optimized spray conditions were further refined in the second DOE conducted in Phase III. The optimal air plasma sprayed process conditions for low resistivity Mo were determined to be: 10 passes of 36 µm Mo sprayed using an arc current of 250 Amps, 34 SLPM Ar and 21 SLPM He gas flows, and standoff distance of 10" or 254mm.

# 6. SUMMARY AND RECOMMENDATIONS

This report documents an effort to prove the feasibility of preparing thermoelectric modules using Air Plasma Sprayed Molybdenum coatings. Molybdenum interconnects were successfully prepared on thermoelectric modules by air plasma spraying a 36µm size Mo powder through a carbon-filled laser-cut Kapton tape mask. The coating had excellent feature spacing and edge retention (~170µm size), was adherent, and exhibited electrical conductivity appropriate for the thermoelectric module application. At the end of the project, Mo interconnects were successfully produced on a thermoelectric module. With the addition of the Ti/Au layer on top of the Mo coating, the module exhibited an electrical resistivity of 128Ω, approaching the theoretical resistivity value of the 6mm leg module of 112Ω.

The Mo coating's electrical resistivity was improved from 301.6 µΩ cm to 47.95 µΩ cm (compare to bulk Mo of 5.5 µΩ cm) through a DOE-based process optimization study. A Mo coating with low electrical resistivity (47.95 µΩ cm) was produced by air plasma spraying at an arc current of 350 Amps, total plasma gas flow of 60.5 SLPM (38.5 SLPM Ar and 22 SLPM He), and standoff distance of 10" or 254mm. This coating was used to prepare Mo interconnects on actual thermoelectric modules. Additional process optimization showed that the electrical resistivity of the Mo coating could be further reduced using the following conditions: arc current of 250 Amps, 34 SLPM Ar and 21 SLPM He gas flows, and standoff distance of 10" or 254mm.

APS coating did not aid in embedding the Ti/Au layer previously sputtered onto the substrate. Thus we recommended that the APS Mo coating be produced first onto the modules, followed by circuit repair, using Ti/Au sputtering.

APS Mo did not show significant chemical reaction with Bi-Te substrate at the coating/substrate interface. Coating microstructure consisted of lamellar splats containing columnar grains, as expected. Round pores (and cracks radiating from the pores) were found immediately under the Mo coating. These pores were associated with tellurium vaporization during the APS process. Vaporization is thought to occur when the molten Mo droplets (2623°C) transferred their heat to the substrate at the moment of impact. We expect that tellurium vaporization can be mitigated by aggressively cooling the substrate during deposition process.

We recommended that liquid $CO_2$ be explored as a substrate cooling method in future studies. This aggressive cooling technique is well known in the spray industry and is expected to mitigate Te vaporization. This capability exists at SNL and can be integrated with the TriplexPro®-210 torch. Cooling the substrate is expected not only to reduce the pores at the coating/substrate interface but also to improve the Mo splat morphology and coating microstructure. We also expect that increased cooling will reduce coating defects and consequently improve the electrical conductivity of the APS Mo coating.

# 7. REFERENCES


1. Satterthwaite, C. B.; Ure, R. (1957). "Electrical and Thermal Properties of Bi2Te3". *Phys. Rev.* **108** (1957): 1164.
2. WolframAlpha; www.wolframalpha.com
3. Davis, J.R.; *Handbook of Thermal Spray Technology*, ASM International, 2005
4. Sulzer-Metco Inc. Technical Bulletin #10-071; Metco® 63 & Metco 63NS Molybdenum Powder
5. *TriplexPro™-210 Plasma Gun Plasma Spraying Product Manual,* MAN105133E01, 02/06/2012; Sulzer-Metco Inc.
6. Van Der Pauw, L.J., "A Method of Measuring Specific Resistivity and Hall Effect of Discs of Arbitrary Shape," *Philips Research Reports* **13** (1958): 1.
7. Blachman, A. "Stress and Resistivity Control in Sputtered Molybdenum films and Comparison with Sputtered Gold," *Metall Trans*. **2** (1971): 699.
8. Mauer, G., Vaßen, R., and Stöver, D. "Detection of Melting Temperatures and Sources of Errors Using Two-Color Pyrometry During In-Flight Measurements of Atmospheric Plasma-Sprayed Particles," *Int. J. Thermophys.* **29** (2008): 764.
9. Rowe, D.M. (ed); *Thermoelectrics Handbook: Macro to Nano*, Taylor and Francis Group, Boca Raton, FL 2006.

# 8. DISTRIBUTION

| | | | |
|---|---|---|---|
| 1 | MS0614 | Daniel Wesolowski | 02545 |
| 1 | MS0959 | Catherine Sobczak | 01832 |
| 1 | MS0959 | Deidre Hirschfeld | 01832 |
| 1 | MS1130 | Aaron Hall | 01832 |
| 1 | MS1130 | Pylin Sarobol | 01832 |
| | | | |
| 1 | MS0899 | Technical Library | 09536 (electronic copy) |

Sandia National Laboratories